

Formation and structure of halos in a warm dark matter cosmology

Vladimir Avila-Reese and Pedro Colín

Instituto de Astronomía, U.N.A.M., A.P. 70-264, 04510, México, D.F., México

Octavio Valenzuela

Astronomy Department, New Mexico State University, Box 30001, Department 4500, Las Cruces,
NM 88003-0001, USA

Elena D’Onghia

Università degli Studi di Milano, via Celoria 16, 20100 Milano, Italy

and

Claudio Firmani

Instituto de Astronomía, U.N.A.M., A.P. 70-264, 04510, México, D.F., México

ABSTRACT

Using high-resolution cosmological N-body simulations, we study how the density profiles of dark matter halos are affected by the filtering of the density power spectrum below a given scale length and by the introduction of a thermal velocity dispersion. In the warm dark matter (WDM) scenario, both the free-streaming scale, R_f , and the velocity dispersion, v_{th}^w , are determined by the mass m_W of the WDM particle. We found that v_{th}^w is too small to affect the density profiles of WDM halos. Down to the resolution attained in our simulations (~ 0.01 virial radii), there is not any significant difference in the density profiles and concentrations of halos obtained in simulations with and without the inclusion of v_{th}^w . Resolved soft cores appear only when we increase artificially the thermal velocity dispersion to a value which is much higher than v_{th}^w . We show that the size of soft cores in a monolithic collapse is related to the tangential velocity dispersion. The density profiles of the studied halos with masses down to ~ 0.01 the filtering mass M_f can be described by the Navarro-Frenk-White shape; soft cores are not formed. Nevertheless, the concentrations of these halos are lower than those of the CDM counterparts and are approximately independent of mass. The cosmogony of halos with masses $\lesssim M_f$ is not hierarchical: they form through monolithic collapse and by fragmentation of larger structures. The formation epoch of these halos is slightly later than that of halos with masses $\approx M_f$. The lower concentrations of WDM halos with respect to their CDM counterparts can be accounted for their late formation epoch.

Overall, our results point to a series of advantages of a WDM model over the CDM one. In addition to solving the substructure problem, a WDM model with $R_f \sim 0.16$ Mpc ($m_W \approx 0.75$ keV; flat cosmology with $\Omega_\Lambda = h = 0.7$) also predicts concentrations, a Tully-Fisher relation, and formation epochs for small halos which seems to be in better agreement with observations relative to CDM predictions.

Subject headings: dark matter — galaxies:dwarf — galaxies:formation — galaxies:halos
— methods:N-body simulations

1. Introduction

The damping of small-scale modes in the power spectrum of density fluctuations has been proposed to overcome potential observational difficulties at small scales of the hierarchical cold dark matter (CDM) scenario for structure formation (e.g., Avila-Reese, Firmani, & Hernández 1998; Moore et al. 1999b; Sommer-Larsen & Dolgov 2000; Hogan 1999; Kamionkowski & Liddle 1999; Hogan & Dalcanton 2000; White & Croft 2000; Colín, Avila-Reese, & Valenzuela 2000). The damping in the power spectrum may be produced either during its primordial generation (in the biased scalar inflationary models, for example) or due to Landau and free-streaming damping, which erase galactic or sub-galactic density fluctuations when the dark matter particles are warm (e.g., Blumenthal, Pagels, & Primack 1982); although the free-streaming damping could also be present in CDM models if CDM particles are non-thermally produced (Lin et al. 2001). In this paper we study warm dark matter (WDM) models; however, it is important to remark that our results are also valid for other models where the power spectrum is damped at small scales.

A potential shortcoming of the CDM scenario, is the large amount of substructure (satellites) that is predicted for Milky-Way like halos with respect to observations under the assumption that at each small halo a dwarf galaxy is formed (Kauffmann et al. 1993; Klypin et al. 1999; Moore et al. 1999a; but see e.g., Bullock, Kravtsov, & Weinberg 2000 for an alternative solution). The cosmological N-body experiments of Colín et al. (2000, hereafter Paper I) have shown that the observed satellite circular velocity function of Milky Way and Andromeda can be reproduced if the power spectrum is exponentially damped (filtered) at scales $\sim 0.1 - 0.2$ Mpc (a flat cosmological model with $\Omega_\Lambda = 0.7$ and $h = 0.7$ was used). A free-streaming scale R_f of $0.1 - 0.2$ Mpc is attained for particle masses m_W of $\sim 0.6 - 1$ keV (Sommer-Larsen & Dolgov 2000). Interestingly, Narayanan et al. (2000) derived a lower limit for m_W of 750 eV from the restriction that the predicted power spectrum should reproduce the observed properties of the Lyman- α forest in quasar spectra.

In Paper I it was also found that the concentrations of satellite WDM halos decrease as R_f increases, being these concentrations lower than those of the corresponding CDM halos. Unfortunately, these small halos were poorly resolved and we could not explore in detail the inner density profiles of halos with masses below M_f . Studying the density profiles of WDM halos with high resolution is necessary, in particular because another potential problem of the CDM scenario is related namely to the inner density profile and concentration of small halos. It seems to be a discrepancy between numerical simulation results and observations of dwarf and low surface brightness (LSB) galaxies (e.g., Moore 1994; Flores & Primack 1994; Burkert 1995; de Blok & McGaugh 1997; de Blok et al. 2001) although other observational studies have challenged this result (van den Bosch

et al. 2000; Swaters, Madore & Trewhella 2000; van den Bosch & Swaters 2000).

In the present paper the density profiles of WDM halos with masses close to or up to ~ 100 times smaller than M_f are studied with a mass resolution 2 – 3 orders of magnitude larger than in Paper I. Our conclusions will be based partly on simulations with a power spectrum corresponding to $m_W \sim 0.6$ KeV. However, in order to study with high resolution the halos with masses below M_f , we need to increase M_f . Thus, we will also use simulations for $m_W \sim 0.13$ KeV ($M_f \sim 10^{14} h^{-1} M_\odot$) and assume that the structure of halos should depend on the halo mass-to- M_f ratio rather than on the specific value of M_f . The cosmogony of halos with masses $< M_f$ is not hierarchical. Halos with masses close to or larger than M_f by factors of 5 – 10 assemble a large fraction of their present-day mass by a coherent and nearly monolithic collapse, whereas halos with masses smaller than M_f form from the gravitational fragmentation of larger pancake-like structures, as in the top-down scenario (Zel’dovich 1970). Firmani et al. (2000b) emphasized that the density profiles of dark halos formed through a monolithic collapse depend significantly on the velocity dispersion of the collapsing particles (see also Aguilar & Merrit 1990); this velocity dispersion may be primordial (thermal relict) or can be acquired during an inhomogeneous gravitational collapse (dynamical).

The non-zero thermal velocities of warm particles (warmons) should produce minimal shallow halo cores because of the phase packing limit (e.g., Gunn & Tremaine 1979). However, this thermal velocity dispersion, v_{th}^w , for warmons with masses of ~ 1 keV seems to be too small to produce a noticeable core (Hogan & Dalcanton 2000). In Paper I this velocity was neglected, leaving uncertain the effect it could have on the structure of simulated halos (Sellwood 2000). Here we will include different thermal velocity values in the simulations in order to explore their influence on the halo density profile. An analytical (dynamical) approach will be also used to study the “hot” monolithic collapse and clarify the conditions required to form shallow cores.

After the completion of this paper, a similar paper by Bode, Ostriker, & Turok (2000) appeared in the preprint list of Los Alamos National Laboratory. Bode et al. study the cosmogony and structure of halos for models with damped power spectra in a cosmological box. They also find that halos with masses below the filtering mass are less concentrated and that these halos form later, relative to CDM. In addition to this, they also describe the spatial distribution and the mass function of these small halos; in this sense, their study complement ours.

In section §2 we present the WDM models to be explored in this paper. In §3 we briefly describe the numerical simulations. In §4 we present the results from our experiments aimed to study the density profiles and concentrations of halos with masses below the mass corresponding to the filtering scale. The influence of the velocity dispersion over the inner density profile of halos formed by monolithic collapse is explored in §5.1. In §5.2 we present results from our WDM cosmological simulations including the thermal velocity dispersion of warmons. In §6.1 we describe and discuss how structure formation proceeds in simulations with a power spectrum suppressed at small scales. The viability of the WDM scenario is discussed in §6.2. Finally, our conclusions are given in §7.

2. Cosmological Models

As in Paper I, here we also use the currently favored flat low-density universe with $\Omega_\Lambda = 0.7$, $h = 0.7$, and $\sigma_8 = 1$, and instead of CDM we introduce WDM. Two characteristics distinguish WDM from CDM: the damping of the small-scale density fluctuations and the fact that thermal velocity dispersion might not be negligible at the time of structure formation. The free-streaming length R_f is related to the mass of the warmon through the following equation (e.g., Sommer-Larsen & Dolgov 2000):

$$R_f = 0.2 (\Omega_{WDM} h^2)^{1/3} \left(\frac{m_W}{1\text{keV}} \right)^{-4/3} \text{Mpc}, \quad (1)$$

where Ω_{WDM} is the contribution to the energy density of the universe from WDM. Modifications to eq. (1) exist; for example, a larger coefficient of proportionality is given by Pierpaoli et al. (1997). Using their coefficient, for a given R_f , m_W should be roughly two times larger than the values used here.

We follow Sommer-Larsen & Dolgov and define a characteristic free-streaming wavenumber k_f as the k for which the WDM transfer function (eq. [4]) is one half; that is, $k_f = 0.46/R_f$. Once R_f has been fixed (this is the “true” input parameter in our simulations), a characteristic filtering mass M_f can be defined conditionally. Unfortunately, this has not been done in an unique way in the literature, introducing some confusion; its value can vary by about three orders of magnitude from one definition to another. For instance, defining M_f simply as $4\pi/3\bar{\rho}_m R_f^3$ gives a value 318 times smaller than the value obtained with the definition given by Sommer-Larsen & Dolgov (2000), which we use in this paper:

$$M_f \equiv \frac{4\pi}{3} \bar{\rho}_m \left(\frac{\lambda_f}{2} \right)^3, \quad (2)$$

where $\lambda_f \equiv 2\pi/k_f = 13.6R_f$. This definition of M_f is justified by the numerical experiments of Tittley & Couchman (1999). They found that the initial density distribution produced by a sharp cut in the power spectrum at $k_c = 2\pi/r_s$ (the exponential drop in the power spectrum in our case is at $k_c = 2\pi/\lambda_f$) is similar to that one produced when the initial density field is convolved with a top-hat window of smoothing radius $\sim r_s/2$. The analysis of the halo properties below shows that the mass at which the WDM halos begin to diverge from the CDM ones is just around the mass given by eq. (2).

We use the WDM power spectrum given in Bardeen et al. (1986):

$$P(k) = T_{WDM}^2(k) P_{CDM}(k), \quad (3)$$

where the WDM transfer function is approximated by

$$T_{WDM}(k) = \exp \left[-\frac{kR_f}{2} - \frac{(kR_f)^2}{2} \right] \quad (4)$$

and P_{CDM} is the CDM power spectrum given by Klypin & Holtzman (1997) (see Paper I).

3. The Numerical Simulations

The simulations were performed using the multiple-mass scheme variant of the Adaptive Refinement Tree (ART) N-body code (Kravtsov, Klypin, & Khokhlov 1997). The ART code achieves high spatial resolution by refining the base uniform grid in all high-density regions with an automated refinement algorithm. The multiple-mass scheme, described in detail elsewhere (Klypin et al. 2000; see also Paper I), is used to increase the mass and spatial resolution in few *selected* halos, which hereafter we will call hosts as in Paper I. However, while in Paper I the host halos were structures much larger than M_f and selected to be relatively isolated, here, in simulations with large R_f , they are smaller than M_f and can be embedded within filaments and can belong to groups at the intersection of filaments. On the other hand, in both CDM and WDM, we call guest halos the bound structures surviving within the virial radii of the host halos. These definitions are more technical than conceptual; note that in the simulations just mentioned above, the host halos contain guest halos, but on their own they may be “guests” of other larger systems.

We start our simulations by making a low mass resolution run with 32^3 or 64^3 particles in a grid with 256^3 cells in which all particles have the same mass. We use these runs to select (host) halos to be re-simulated with higher mass and force resolution. We then identify all particles within ~ 2 virial radii and trace them back to get their Lagrangian positions at $z = 40$. For the cosmology used in this paper, the virial radius r_v is defined as the radius within which the average halo density is 334 times the background density, according to the spherical collapse model. Next, the initial distribution with particles with different masses is generated and the models are evolved to the present time with the multiple-mass variant of ART. Models with $R_f = 0.2$ Mpc have four mass levels (particles with masses 1, 8, 64, $256 \times m_p$) whereas models with $R_f = 1.7$ Mpc have three levels. The mass resolution on the finest mass level corresponds to a box of 256^3 particles in both series of simulations.

As in Paper I, the Bound Density Maxima (BDM) group finding algorithm was used to locate the host halos in the low mass resolution run. The BDM algorithm finds the positions of local maxima in the density field smoothed at the scale of interest and applies physically motivated criteria to test whether a group of particles is a gravitationally bound system. The BDM is also used to find the host and the guest halos in the multiple-mass high resolution simulations.

In Table 1 we present an overview of all the simulations used in this paper. The formal force resolution shown in column 6 is the size of a cell in the finest refinement grid, and the mass per particle (column 4) is the mass for those particles which belong to the finest level of mass resolution. The halo density profile can be studied with high confidence only for radii larger than ~ 4 times the formal force resolution (Klypin et al. 2000) and containing within them more than 50-100 particles.

The first set of runs in Table 1 was aimed at studying in detail the density profiles and concentrations of halos with virial masses close to or below the corresponding filtering mass M_f . Model Λ WDM is the same simulation presented in Paper I for $R_f = 0.2$ Mpc but run in a smaller box, $L_{\text{box}} = 7.5 h^{-1}\text{Mpc}$, in order to attain more mass resolution. The host halo studied in this run

is 1.7 times less massive than the same halo in the run with $L_{\text{box}} = 15h^{-1}\text{Mpc}$.¹ Unfortunately, in the simulation with the box size reduced, the most massive guest halos turned out to be small, containing less than 1000 particles.

Since it is not easy to know the masses of the guest halos *a priori*, and since our aim is just to explore the density profiles of halos with masses smaller than M_f , a better strategy is to study halos in simulations where we select them *a priori* (hosts), with the desired masses below M_f . Although from the technical point of view of our approach these halos are hosts, they may be well embedded within larger halos, i.e., they could be satellites (guests). We set $R_f = 1.7 \text{ Mpc}$ which corresponds to $M_f = 1.7 \times 10^{14} h^{-1}M_{\odot}$, and re-simulate with high resolution smaller and smaller host halos in runs with decreasing box sizes. For this model ($m_W=125 \text{ eV}$), the structure formation process is close to the hot dark matter regime. Nevertheless, in the assumption that the formation and structure of halos depend on M_v/M_f rather than the specific value of M_f , this model will give guidance to the physics on smaller scales in a model with a more realistic warm mass. We think this assumption is plausible. In any case, general trends can be compared with the (low resolution) results from simulations with $m_W=605 \text{ eV}$.

Runs $\Lambda\text{WDM}_{7.5}$, ΛWDM_{15} , ΛWDM_{30} , and ΛWDM_{60} (Table 1), are for $L_{\text{box}} = 7.5, 15, 30$ and $60 h^{-1}\text{Mpc}$, respectively. For comparison, we also run a CDM simulation ($R_f = 0$) with the same initial condition as ΛWDM_{60} (run ΛCDM_{60}). In model ΛWDM_{60} we re-simulated four host halos with masses 2 – 4 times smaller than M_f . They were resolved with $\sim 4 - 7 \times 10^4$ particles. In order to obtain halos with masses even ~ 10 times smaller but with the same mass resolution, we reduced the box size by a factor of two. This is run ΛWDM_{30} , where four halos with masses 22 – 33 times smaller than M_f were re-simulated. In run ΛWDM_{15} , the only host halo re-simulated is already 45 times smaller than M_f and has 3.54×10^5 particles. The guest halos (those contained within the virial radii of hosts) in all of these simulations have masses smaller than $\sim 0.01 M_f$ and are resolved with $\lesssim 7000$ particles. Finally, in run $\Lambda\text{WDM}_{7.5}$ the selected halo is 300 times less massive than M_f and it is resolved with 2.73×10^5 particles.

At this point, it is important to note the effect that a reduction of the box size has on the results from WDM simulations. In CDM simulations we do not expect that a reduction in the box size affects the internal structure of halos with radii much smaller than L_{box} (e.g., Frenk et al. 1988). However, in WDM simulations the loss of long wavelengths may critically affect the formation and the structure of halos if the fundamental wavelength ($= L_{\text{box}}$) is close to or smaller than the characteristic filtering wavelength λ_f . When dealing with WDM power spectra, one should keep in mind that structures of scales smaller than $\sim \lambda_f$ arise from a transfer of power from large to small scales (see §6.1). Hence, if the large scale modes are omitted, especially those around the peak, then the formation of small structures becomes affected. For CDM this is not a problem

¹This is in fact what we find in all of our WDM experiments: the mass of a given halo becomes smaller as L_{box} is reduced. However, this mass reduction is not dramatic, and we do not expect it will change our conclusions about concentrations and density profiles of the halos, because they both are not typically very dependent on mass.

because small scales have ever more power than the large ones and the structure formation process is dominated by the smallest scales.

Since the filtering wavelength for $R_f = 1.7$ Mpc is $\lambda_f = 16h^{-1}\text{Mpc}$ (see §2), run ΛWDM_{15} is at the limit of confidence while for run $\Lambda\text{WDM}_{7.5}$, the mode corresponding to the peak of the WDM power spectrum is absent (the fundamental mode lies beyond the peak). The density profile of the halo re-simulated in this peculiar model (a narrow and exponentially damped power spectrum) indeed strongly deviates from profiles of halos obtained in other WDM simulations with larger box sizes as will be seen in §4.

The second set of simulations shown in Table 1 was aimed at studying the effect that a warm non-zero thermal velocity, v_{th}^{w} , has on the internal structure of simulated halos. From this study we conclude that v_{th}^{w} does not affect the inner density profile of WDM halos, at least down to the scale at which we are confident of the resolution of our simulations ($\sim 0.01r_v$). Run $\Lambda\text{WDM}_{\text{t}2}$ is the same as ΛWDM ($R_f = 0.2$ Mpc) but introducing a thermal velocity component twice larger than v_{th}^{w} . Runs $\Lambda\text{WDM}_{60\text{t}2}$, $\Lambda\text{WDM}_{60\text{t}4}$, and $\Lambda\text{WDM}_{60\text{t}16}$, are the same as ΛWDM_{60} ($R_f = 1.7$ Mpc) but introducing thermal velocities with amplitudes 2, 4 and 16 times larger than the corresponding v_{th}^{w} .

In order to attain a visual impression of how structure formation does proceed for models with a damped power spectrum, we present in Fig. 1a snapshots at different epochs of the run ΛWDM_{60} . The figure snapshots show the distribution of particles inside a cube of $40 h^{-1}\text{Mpc}$ comoving on a side. The center of each cube is the center of mass of the particles that were traced back to the selected epoch from a sphere of radius $1.5 h^{-1}\text{Mpc}$ centered in one of the host halos at $z = 0$ (Fig. 1c, see below). In Figure 1b we show the same as in Fig. 1a, but for the corresponding CDM model, run ΛCDM_{60} . The different formation histories of halos with masses $\approx M_f$ or below in models with and without damped power spectra are highlighted in these two panels; in particular, we notice that these halos (i) form later in model ΛWDM_{60} than in ΛCDM_{60} (the amount of substructure at $z \sim 2$ in model ΛWDM_{60} is reduced to a solitary sharp filament) and (ii) that they are only located within filaments in the WDM case while in the CDM one, they can also be found outside the filaments (see also Bode et al. 2001). In Fig. 1c we show a zoom of the central region of plot 1a at two times, $z = 1$ and $z = 0$. In the right panel all particles inside a sphere of $1.5 h^{-1}\text{Mpc}$ centered on a host halo at $z = 0$ are plotted. The mass of this halo is about half the filtering mass ($M_f = 1.7 \times 10^{14} h^{-1}M_\odot$) and it was one of the first structures to collapse in the simulation. In the left panel, the particles plotted in the right panel were traced back to $z = 1$. Note that the virialized halos seem to emerge from the filamentation and fragmentation of pancakes. In any case, the detailed study of halo formation in WDM-like models is beyond the scope of this paper.

An effect that is becoming typical of cosmological high-resolution simulations with damped power spectra is the finding of relatively small halos regularly spaced in filaments. An example of this is shown in Fig. 1a at $a = 0.5$; see those knots that lie inside the filament which points from right to left to the center of the cube. Several of these knots were indeed selected by our

halo finding algorithm as self-gravitating structures. The space regularity, also seen in other of our simulations, make us to suspect that the origin of these very small halos with respect to M_f may be a numerical artifact attributed perhaps to finite grid effects. A detailed study of this effect is highly desirable since it might produce an steepening of the circular velocity function distribution of satellites at the small velocity end.

4. Density profiles of halos with masses near or below the filtering mass

In Paper I host halos of a few $10^{12}h^{-1}M_\odot$ were re-simulated using the multiple-mass scheme in a box size of $15 h^{-1}\text{Mpc}$ for a ΛCDM model with $R_f = 0.2 \text{ Mpc}$. The mass per particle in the finest level of resolution corresponded to $1.66 \times 10^7 h^{-1}M_\odot$. Thus, the guest halos reported in Paper I (with scales below the filtering scale) were poorly resolved; they only had a few 10^2 particles, a number not high enough to study in detail their inner density profiles. As mentioned in §3, we also run the same simulation of Paper I but with the box size reduced by a factor of two (run ΛWDM). We find that the most massive guest halos are smaller than the most massive ones from the $15 h^{-1}\text{Mpc}$ run, in such a way that they were resolved with not much more particles than in Paper I. Figure 2 (upper panel) shows the density profiles of the host and guest halos with more than 1000 particles (the latter were shifted vertically in order to avoid too much overlapping). The radius of the innermost point is at least four times the formal force resolution and contains more than 50 particles within it (see §3; this criteria applies for all density profiles shown in this paper). For the host halo, the innermost radius is $4 \times 0.1 h^{-1}\text{kpc}$, and for the guest halos is $\approx 1.2 h^{-1}\text{kpc}$. As one sees from Figure 2, the density profiles of guest halos — whose masses are ~ 0.01 times smaller than the filtering mass $M_f = 2.8 \times 10^{11} h^{-1}M_\odot$ — are well described by the Navarro, Frenk, & White (1997, NFW) profile (dashed lines), from ~ 0.04 to $1 r_v$.

As described in §3, for a series of ΛWDM simulations with $R_f = 1.7\text{Mpc}$ and different box sizes, we re-simulated with high resolution selected halos (hosts) with masses smaller than the corresponding $M_f = 1.7 \times 10^{14} h^{-1}M_\odot$, obtaining in this way halos with a large number particles.

In Fig. 3 we show the density profiles of the host halos with masses 2 – 4 times smaller than M_f from run ΛWDM_{60} (filled circles) and those obtained in the same simulation but with CDM instead of WDM (run ΛCDM_{60} , empty circles). Although both simulations started with identical phases (seeds) and large scale normalization, the CDM halos are slightly more massive than the corresponding WDM ones (by factors $\sim 1.1 - 1.4$). The dashed lines are the NFW fit to the plotted profiles. As can be seen from this figure, the NFW shape describes rather well the density profiles of both the WDM and CDM halos, for radius ranging from ~ 0.01 to $1 r_v$, although in the innermost parts, the slope tends to be steeper than r^{-1} , in particular for the CDM halos (Moore et al. 1999a). The accuracy of the fit can be estimated with the parameter $D \equiv \chi^2/N$, where $\chi^2 = \sum_i^N [\log(\rho_i/\rho_{an})]^2$ (ρ_i and ρ_{an} are the measured and analytical values of the density, respectively) is the quantity used for minimization of the fitting, and N is the number of radial bins (points to fit). For the host halos in runs ΛWDM_{60} and ΛCDM_{60} , on average $D \approx 6.5\%$ and

5.5%, respectively.

In order to explore the structure of halos with masses much smaller than M_f , we have run simulations with the same $R_f=1.7$ Mpc but with box sizes of 30, 15 and $7.5 h^{-1}$ Mpc (runs Λ WDM₃₀, Λ WDM₁₅, and Λ WDM_{7.5}, respectively); in these simulations we re-simulate host halos with masses of $\approx 6 - 95 \times 10^{11} h^{-1}M_\odot$. Note that these halos may be embedded within larger halos, i.e. they could be satellites (see §3 for the technical definitions of host and guest halos).

Figure 4 shows the density profiles of the four host halos obtained in the run Λ WDM₃₀ (upper panel), and of the two host halos obtained in runs Λ WDM₁₅ and Λ WDM_{7.5} (lower panel). For comparison, the density profile of a CDM halo of $2.5 \times 10^{12} h^{-1}M_\odot$ presented in Paper I is also plotted (empty circles). Though now the masses of the halos are up to ~ 50 times smaller than M_f , the NFW fit (dashed lines) continues to be a good description for the density profiles of WDM halos explored with accuracy down to $\sim 0.01 r_v$. The deviation parameter D is on average $\sim 6\%$ for host halos from run Λ WDM₃₀ and $\sim 3.5\%$ for the only host halo from run Λ WDM₁₅. Nonetheless, the WDM halos are less concentrated and shallower in the center than their CDM counterparts.

The density profile of the host halo from simulation Λ WDM_{7.5} shows a prominent shallow core and a disturbed outer density profile. As this run has a box size already smaller than the filtering wavelength λ_f , it samples only the high-frequency drop of the WDM power spectrum; we thus expect the inner structure of the formed halo to be significantly affected (see §3).

The results obtained here confirm our previous result: the WDM halos with masses near or below the filtering mass are *less concentrated* than the corresponding CDM halos (Paper I). In Figure 5a we plot the $c_{1/5}$ concentration parameter² versus virial mass M_v for the host halos from the different runs with $R_f = 1.7$ Mpc. We also include in this plot guest halos with more than 1000 particles. They are only a few and their inner density profiles are resolved only down to $\sim 0.03 r_v$. The concentrations and inner density profiles of surviving guest halos are not expected to be significantly affected by the fact that they are within larger systems. In fact, some of the host halos in the different runs are also within larger halos. Results for the WDM model with $R_f = 0.2$ Mpc are also shown in Fig. 5a: crosses are from Paper I and skeletal triangles correspond to the Λ WDM run presented here. Halos with less than 90 particles were excluded.

In order to compare the concentrations of WDM and CDM halos, we also plot in Fig. 5a the results from our Λ CDM simulation of box size $60 h^{-1}$ Mpc (empty circles) as well as a linear fitting for thousands of isolated and clustered halos found in a Λ CDM simulation (Avila-Reese et al. 1999). The trend in Fig. 5a is clear: as the halo mass becomes smaller than M_f , the $c_{1/5}$ concentration departs more and more from the corresponding CDM concentration. Although the dispersion in the concentration is big (see Fig. 8 in Avila-Reese et al. 1999 and Fig. 8 below)

²The concentration $c_{1/5}$ is defined as the ratio between the virial radius r_v and the radius where 1/5 of the total halo mass is contained (Avila-Reese et al. 1999). This definition of the concentration parameter is independent of the particular fitting applied to the halo density profile.

the trend seen in Fig. 5a for the WDM halos is clear and is out of the statistical dispersion of the $c_{1/5}-M_V$ relation of the CDM halos. For completeness, the concentrations obtained when fitting the density profiles of the halos to a NFW profile (c_{NFW}) are also presented in panel (b) of Fig. 5 (only halos with $D < 10\%$ were included). The four halos from the $60 h^{-1}\text{Mpc}$ CDM simulation, as well as a linear interpolation for the $c_{\text{NFW}} - M_V$ relation obtained from the ΛCDM simulation presented in Avila-Reese et al. for halos whose density profiles are well described by the NFW shape, are also shown in this plot.

5. Effect of thermal velocity dispersion on the density profile

There are two relevant conditions for the problem of halo formation, namely the initial fluctuation density profile —which determines the kind of collapse the halo suffers— and the amplitude of the (tangential) velocity dispersion v_{rms} of the collapsing particles. The CDM halos form hierarchically and the v_{rms} is acquired *dynamically* since early epochs due to interactions of substructures with the global tidal field. In a WDM scenario, the first structures to collapse are those with masses close to M_f ; they assemble the mass M_f almost synchronously followed by some mass accretion (quasi-monolithic collapse). It is possible that structures formed by fragmentation also suffer a quasi-monolithic collapse. As the collapse of halos less massive than M_f is delayed and the amount of substructure is small (compared to halos formed hierarchically), one expects that particles will acquire a lower tangential velocity dispersion than in the hierarchical case, although this is a question to be explored in the numerical simulations. Instead, WDM particles have an intrinsic (residual) *thermal* velocity dispersion.

An interesting question to explore is how the angular momentum of the particles — due to either a residual thermal velocity or to a v_{rms} acquired dynamically — affects the inner structure of virializing systems. For halos formed hierarchically, the velocity dispersion is not relevant for the formation of a soft core (e.g. Avila-Reese et al. 1998; Huss, Jain, & Steinmetz 1999), but for halos formed monolithically it may be. In §5.1 we present an *heuristic* (analytical) model of halo virialization which allows us to understand the role that velocity dispersion plays in a monolithic collapse. We will also find an expression to relate the soft core radius with v_{th} , using N-body simulations for hot monolithic collapse and virialization. In §5.2 results from cosmological N-body simulations, including several values of v_{th} , will be presented.

5.1. Thermal monolithic collapse and soft cores

Let us study the monolithic collapse of a sphere of mass M , radius R_M , and uniform density ρ_M at maximum expansion. We can introduce some thermal energy assuming that all particles move on elliptical orbits with a given eccentricity e . The constancy of the density and e with radius assure that all particles have the same orbital period τ and that the pericenter-to-apocenter ratio

is the same for all of them, respectively. Therefore, shell crossing is avoided. For purely radial motion, ($e = 1$), the collapse reaches a singular point. For $e < 1$, at maximum concentration, i.e. when each particle is found at pericenter, the collapse leads to a uniform sphere with radius

$$r_c = R_M(1 - e)/(1 + e). \quad (5)$$

The existence of this maximum concentration state is at the base of the existence of a soft core in the virialized halo. Tangential velocity at apocenter is:

$$v_t^2 = \frac{r^2 4\pi G \rho_M (1 - e)}{3}, \quad (6)$$

while, at the maximum expansion, the total thermal energy T and the potential energy W are given by:

$$T = \frac{8\pi^2 G \rho_M^2}{15} (1 - e) R_M^5 \quad (7)$$

$$W = \frac{16\pi^2 G}{15} \rho_M^2 R_M^5, \quad (8)$$

where the relationship between e , T and W is: $2T/W = 1 - e$.

The simplest approximation to estimate the virialized density at a given radius (density profile) is to assume a time average density at the same radius. This approach is based on the statistical hypothesis that the time average density is representative of the virialized halo density. Using the conventional motion parametric equations:

$$\begin{aligned} r &= \frac{R_M}{(1 + e)} (1 - e \cos \theta) \\ t &= \sqrt{\frac{3}{4\pi G \rho_M (1 + e)^3}} (\theta - e \sin \theta), \end{aligned} \quad (9)$$

the time average density at a radius r between r_c and R_M is:

$$\begin{aligned} \langle \rho(r) \rangle &= \frac{\int_0^\tau \rho(r, t) dt}{\int_0^\tau dt} = \frac{\rho_M (1 + e)^3}{\pi} \int_{\theta_c}^\pi \frac{1}{(1 - e \cos \theta)^2} d\theta = \\ &= \frac{\rho_M (1 + e)^3}{\pi (1 - e^2)} \left[\frac{\pi}{\sqrt{1 - e^2}} - \frac{\sqrt{e^2 - \eta^2}}{1 - \eta} - \frac{2}{\sqrt{1 - e^2}} \tan^{-1} \left(\frac{1 + e}{\sqrt{1 - e^2}} \sqrt{\frac{e - \eta}{e + \eta}} \right) \right], \end{aligned} \quad (10)$$

while between 0 and r_c (the soft core) the average density is:

$$\rho_c = \rho_M \left(\frac{1 + e}{1 - e} \right)^{3/2} \quad (11)$$

where $\eta = 1 - (1 + e)r/r_0$ and $\cos \theta_c = \eta/e$. The constant density between 0 and r_c is product of the *particle angular momentum which prevents the particles from reaching the center*. The core mass is given by:

$$M_c = M \left(\frac{1 - e}{1 + e} \right)^{3/2}. \quad (12)$$

Equations (5), (11), and (12) clearly show that the ellipticity of the orbits is at the basis of the soft core formation in a monolithic collapse.

From our analysis, we conclude that soft cores in virialized dark collisionless halos may result only from two simultaneous conditions: (1) an initial homogeneous density profile for the progenitor of the present structure (monolithic collapse), and (2) the presence of velocity dispersion with a tangential component. The angular momentum of kinetic motion avoids the migration of particles toward the center, limiting the central density.

In order to obtain a more quantitative relation between the core radius r_c and the velocity dispersion v_{rms} , we resort to N-body simulations of monolithic spherical (top-hat) collapse with several values of v_{rms} injected uniformly at the maximum of expansion. The public version of HYDRA, an adaptive P3M-SPH code (Couchman, Thomas & Pearce 1995), was used. The simulations can be rescaled to any mass M and radius at maximum expansion R_M through the following relations: $M = m\hat{M}$, $R_M = r\hat{R}_M$, $t = (r^3/m)^{0.5}\hat{t}$, and $v_{\text{rms}} = (m/r)^{0.5}\hat{v}_{\text{rms}}$, where m and r are scaling parameters and the quantities with a hat are obtained in the simulation. We will assume that \hat{v}_{rms} is related to a relict thermal velocity \hat{v}_{th} , which decays adiabatically as $\hat{v}_{\text{th}} \propto \hat{R}^{-1}$ until the sphere attains its maximum expansion, $\hat{R} = \hat{R}_M$. We give \hat{v}_{th} when the fluctuation is still in its linear regime and calculate its value, $\hat{v}_{\text{th},M}$, at the maximum of expansion of the sphere of mass \hat{M} . The latter is the stage from which we start the N-body simulation.

From a set of simulations with $\hat{M} = 3.1 \times 10^{11} M_\odot$ (1.64×10^4 particles) and $\hat{R} = 0.5$ Mpc, we have found how the core radius scales with the injected velocity dispersion. The softening radius is 500 pc. We define the core radius r_c as the radius where the central density decreased by a factor of 3. In Fig. 6 we show the results from simulations of hot monolithic collapse (open triangles) and the results of the analytic model presented above (continuous and dashed line). The line is valid for high tangential velocity dispersion when shell crossing effects are negligible. When $\hat{v}_{\text{th}} \lesssim 6$ km s $^{-1}$, the linear relation $\hat{r}_c \approx 3[\text{kpc}]\hat{v}_{\text{th}}$ is a good approximation. Using the scaling relations mentioned above and the expression $R_M = [(32GM)(H_0^2\Omega_m 9\pi^2)]^{1/3}/(1+z_M)$ valid approximately for a top-hat sphere in a flat low-density universe, we obtain:

$$r_c \approx \frac{2.5h^{-1}\text{kpc}}{\sqrt{\Omega_{m,0.3}}} \frac{v_{\text{th},M}/\text{km s}^{-1}}{(1+z_M)^{3/2}}. \quad (13)$$

The applicability of this formula is valid only for $v_{\text{th},M} \lesssim 2\text{km s}^{-1}\Omega_{m,0.3}^{1/6}(hM_{10})^{1/3}(1+z_M)^{1/2}$, where M_{10} is the mass in units of $10^{10}M_\odot$. In the Λ WDM case, z_M refers to the redshift of maximum expansion of structures with masses close to M_f , and $v_{\text{th},M}$ refers to the relict thermal velocity dispersion these structures have at z_M . Note that the upper limit velocity given above is by much larger than the corresponding v_{th}^w . If the less massive halos, which form by fragmentation, also suffer a monolithic collapse at a redshift not much later than z_M (see §6.1), then their thermal core radii also can be roughly predicted with eq. (13). Equation (13) is easy understood on the light of the angular momentum analysis of Bode et al. (2000).

For a Λ WDM model with $m_W=0.6$ KeV, then $M_f = 2.8 \times 10^{11} h^{-1} M_\odot$ and $v_{\text{th}}^w=3.5$ km s $^{-1}$ at

$z = 40$. According to the spherical top-hat model and using the respective Λ WDM variance, the maximum expansion redshift for a $M_f = 2.7 \times 10^{11} h^{-1} M_\odot$ 2σ (1σ) fluctuation is $z_M = 5.3$ (2.1). At this redshift the thermal velocity of the top-hat sphere decreased adiabatically to $v_{\text{th},M} = 1 \text{ km s}^{-1}$ (0.5 km s^{-1}). Then, according to eq. (13), the core radius of halos with masses close to M_f is $r_c \approx 150 \text{ pc}$ (215 pc). This radius should be approximately the same for smaller halos, unless these halos during the fragmentation process acquire large velocity dispersions. Therefore, the thermal soft cores in WDM models are only a very small fraction of the virial radius, at least for halos not much smaller than M_f .

5.2. Results from N-body simulations

Previous estimates showed that the warmion relic velocity dispersion v_{th}^w is too small to influence the halo inner density profiles. Now we resort to cosmological simulations which include several values of v_{th} in order to explore this question. For a warmion of $\sim 1 \text{ keV}$, v_{th}^w is small (at $z = 40$, $v_{\text{th}}^w \sim 2 \text{ km s}^{-1}$ which is about 10 times smaller than the typical peculiar velocities at that epoch). A larger thermal velocity dispersion could be possible if warmions self-interact; in this case the same free-streaming scale R_f can be attained with a smaller particle mass (Hogan 1999; Hannestad & Scherrer 2000) and, since $v_{\text{th}}^w \propto m_W^{-4/3}$, a smaller m_W implies a larger v_{th}^w . According to Hannestad & Scherrer (2000), the mass of the warmions that produce a given free-streaming scale in the case of collisionless WDM could be 1.9 times smaller if warmions self-interact. Therefore, the thermal velocity dispersion could be up to 2.3 times larger in the latter case.

We have run two of the simulations presented in §3 (runs Λ WDM and Λ WDM₆₀) introducing a thermal velocity component in the particles with several amplitudes. The thermal velocities were randomly oriented and their magnitudes were drawn from a Fermi-Dirac phase space distribution with a given rms velocity v_{th} . These velocities were added to the initial peculiar velocities computed using the Zel'dovich approximation.

For our preferred model ($R_f=0.2 \text{ Mpc}$), we compare the $c_{1/5}$ concentrations obtained in runs Λ WDM ($v_{\text{th}}=0$) and the same model but with v_{th} twice higher than v_{th}^w , the warmion velocity corresponding to the given R_f value (Λ WDMt2), making echo of the paper by Hannestad & Scherrer cited above. In Fig. 7 we plot $c_{1/5}$ versus M_v for the only host halo and the more than a dozen guest halos obtained in both simulations at two different epochs, $z = 0$ and $z = 1$. There is not any obvious difference, in the concentrations of halos from both runs. The density profiles of the host and guest halos with more than 1000 particles from run Λ WDMt2 are shown in the lower panel of Fig. 2. As can be seen from Figs. 2 and 7, the introduction of a relic velocity dispersion, even two times higher than v_{th}^w , does not affect notably the structure of WDM halos, at least in the parts where we attain good resolution (down to $\sim 0.04 r_v$).

In order to explore in more detail the effect of v_{th} on the inner halo structure, we have run model Λ WDM₆₀ (its resolution is $\sim 0.01 r_v$) with an ever increasing v_{th} . In runs Λ WDM₆₀t2, Λ WDM₆₀t4,

and $\Lambda\text{WDM}_{60\text{t}16}$, v_{th} was fixed to values 2, 4 and 16 times larger than the v_{th}^{w} corresponding to a warmon of mass 125 eV ($R_f=1.7$ Mpc), respectively. For the latter case, the thermal velocities at $z = 40$ are ~ 7 times higher than the peculiar velocities. Figure 8 shows the density profiles for the four host halos (shifted vertically by -1 in the log) obtained in the series of runs ΛWDM_{60} , $\Lambda\text{WDM}_{60\text{t}2}$, $\Lambda\text{WDM}_{60\text{t}4}$, and $\Lambda\text{WDM}_{60\text{t}16}$. While for the simulations with $v_{\text{th}}= 2$ and 4 times v_{th}^{w} the inner density profiles still do not deviate significantly from the case with $v_{\text{th}}=0$, in the simulation with $v_{\text{th}} = 16v_{\text{th}}^{\text{w}}$, a soft core is already evident at radii smaller than $\sim 0.03 - 0.04 r_v$.

The redshifts at maximum expansion of the four halos from runs $\Lambda\text{WDM}_{60\text{t}2}$, $\Lambda\text{WDM}_{60\text{t}4}$, and $\Lambda\text{WDM}_{60\text{t}16}$, are roughly 1.7 – 1.3. Therefore, the core radii predicted with eq. (13) for these halos are approximately 3.6 – 3.9, 7.2 – 7.8 and 28.6 – 31.4 $h^{-1}\text{kpc}$, respectively. Halos in the last two runs have roughly $r_c = 10 - 15 h^{-1}\text{kpc}$ and $r_c = 31 - 33 h^{-1}\text{kpc}$, respectively. One should take into account that in the cosmological simulations, the studied halos do not suffer a perfect monolithic collapse, and that some velocity dispersion can be acquired during the collapse of the pancakes and filaments.

In conclusion, the introduction of a warmon relict thermal velocity has no any important effect on the density profiles and concentrations of WDM halos. This velocity would have to be much larger in order to produce noticeable soft cores, as eq. (13) shows. We should note that simulations with and without a thermal velocity are not similar at all. The identity of the guest halos is not the same for all of them and their spatial distribution is different in both simulations. However, in a statistical sense, neither the concentrations nor the satellite circular velocity function change.

6. Discussion

6.1. The formation of low-mass halos in simulations with a damped power spectrum

When the power spectrum of fluctuations is damped above some wavenumber k_f , “pancakes” of size $\sim k_f^{-1}$ are the first structures to collapse and smaller objects are expected to form later by fragmentation (e.g., Zel’dovich 1970; Doroshkevich et al. 1980). The coupling between different modes in the non-linear gravitational evolution drives a transfer of power with power flowing from larger to smaller scales. This transfer is very efficient; numerical simulations confirmed previously such a behavior (e.g., Little, Weinberg, & Park 1991; Bagla & Padmanabhan 1997; White & Croft 2000).

Although our numerical experiments were not aimed at studying the structure formation process in a statistical sense (for this see Bode et al. 2000), we noticed that indeed the first structures to collapse are those with scales close to the filtering scale length λ_f . These structures form smooth coherent filaments when they enter the non-linear regime (Fig. 1a; see also Melott & Shandarin 1990; Little et al. 1991, and more references therein) instead of the chains of dense clumps seen in CDM simulations (Fig. 1b).

In the left panel of Fig. 1c one may appreciate the filamentary structure of the protohalo that at $z = 1$ is becoming non-linear. This structure collapses roughly at the same time (quasi-monolithic collapse) but obviously the initial conditions are not spherically symmetric. Nonetheless, matter flows towards the center of the filament and some spherical symmetry is established there (see the virialized halo at $z = 0$). Within the shrinking filament, substructure probably forms by fragmentation. Theoretical and numerical support to the idea that cosmological pancakes are unstable with respect to fragmentation and the formation of filaments can be found in Valinia et al. (1997), and more references therein.

Based on a visual inspection (see also Table 2 and discussion below), we may say that the collapse of the substructure within the filament is almost parallel to the collapse of the filament. As mentioned above, the power transfer from larger to smaller scales is very efficient. It also seems that the collapse epoch of the fragmented halos is independent of their masses. Nevertheless, all these halos collapse on average later than in a CDM simulation. This might explain why the small WDM halos are less concentrated and why their concentrations, though with a large scatter, do not depend on mass (see Fig. 5). Because halos are less concentrated than in the CDM simulations, they are more easily disrupted. As was shown in Paper I, the reduction of the number of small halos due to this effect is comparable to the effect that the power spectrum suppression has on this number, and both work together to deliver a very small number of satellites at $z = 0$.

Interestingly, our results suggest that on average and in a first approximation, the density profiles of dark matter halos are indeed universal, no matter how they form, either by hierarchical clustering or by a monolithic collapse or by fragmentation (see also Moore et al. 1999b). The difference seen in their concentrations can be explained just as an *effect of the formation epoch, which for small WDM halos is delayed compared to the formation epoch of their CDM counterparts*. As we have shown in §5, a way to affect significantly the inner density profile of halos in the case of a monolithic collapse is by including a high (tangential) velocity dispersion. The thermal velocities of warmons of mass ~ 1 keV are much smaller than this required velocity dispersion.

6.2. Viability of the WDM scenario: observational tests

Because of the increasing evidence that the predictions of the nowadays standard Λ CDM model at small scales are in conflict with observations, modifications to this scenario, *able to retain their successful predictions at large scales*, have been recently analyzed. As the nature of dark matter particles is still a mystery, it is tempting to exchange CDM particles for WDM particles as the most simple modification to the standard scenario. At least from the point of view of the particle physics, there is not an obvious preference for any of these particles (e.g., Colombi, Dodelson, & Widrow 1996). But, what are the advantages of the WDM scenario with respect to the CDM one from the point of view of structure formation? Following, we present a list of what we consider are these advantages:

1. For a WDM model with $R_f \gtrsim 0.1$ Mpc ($m_W \lesssim 1$ KeV), $\Omega_m = 0.3$, and $\Omega_\Lambda = h = 0.7$, the observed maximum circular velocity function of Milky Way and Andromeda satellites is roughly reproduced (Paper I).

2. Although in the WDM scenario the halos with masses close to or below M_f do not have a noticeable constant density core, they are less concentrated and have a density profile shallower in the center than their CDM counterparts (§§4 and 5). Recent observational studies have shown that with the current data is not possible to accurately constrain the halo inner density profiles of dwarf and LSB galaxies; these profiles are probably not steeper than r^{-1} and, if anything, the concentrations of these halos are lower than those predicted in the CDM scenario (van den Bosch et al. 2000; Swaters, Madore & Trewheella 2000; van den Bosch & Swaters 2000). In Fig. 9 we compare the $c_{1/5}$ concentration of guest WDM halos from runs Λ WDMt2 and Λ WDM with the $c_{1/5}$ concentration of dwarf and LSB galaxies, inferred from observational data (see details in the figure caption). Unfortunately, there is not an overlap between the theoretical and observational data; nonetheless, it can already be appreciated that the guest WDM halos are in better agreement with observations.

3. The formation of disks within WDM halos ($m_W \lesssim 1$ keV) in N-body+hydrodynamic simulations does not seem to suffer from the disk angular momentum problem (Sommer-Larsen & Dolgov 2000). This problem is also at the basis of other difficulty reported by Steinmetz & Navarro (1998): the predicted infrared Tully-Fisher (TF) relation in their simulations is much brighter than the observed one. The maximum circular velocity V_{\max} of the system increases after disk formation. In the numerical simulations of Steinmetz & Navarro this increase is about a factor of two larger than for models where detailed angular momentum conservation is assumed for the infalling gas (e.g., Mo, Mao, & White 1998; Avila-Reese et al. 1998; Avila-Reese & Firmani 2000; Firmani & Avila-Reese 2000). A factor of two in the velocity translates into a factor of ~ 8 in mass or luminosity explaining why Steinmetz & Navarro obtain a brighter TF relation. If the angular momentum problem is alleviated as in the WDM scenario, then one expects that the zero-point of the TF relation predicted in numerical simulations will be in agreement with observations (Sommer-Larsen & Dolgov 2000).

4. Several authors have shown that the TF relation of normal disk galaxies in the infrared band is an imprint of the mass-velocity ($M_v - V_{\max}$) relation of CDM halos (Firmani & Avila-Reese 2000 and more references therein). For masses larger than $\sim 10M_f$, there are not major differences between the CDM and the WDM halos (Paper I; see also Avila-Reese et al. 1998). How does the $M_v - V_{\max}$ relation look for small masses? In Fig. 10 we have plotted M_v versus V_{\max} for our WDM models with $R_f = 0.2$ Mpc. We also show in this figure the $M_v - V_{\max}$ relation of guest halos obtained for a Λ CDM simulation, its scatter and a linear fit to this relation (Avila-Reese et al. 1999). As expected, the WDM halos move towards the lower V_{\max} side. The formation of dwarf galaxies may be strongly affected by feedback and reionization; these galaxies could lose some of their initial baryon matter through galactic winds (e.g., Mac Low & Ferrara 1999) or through photo-evaporation (Shapiro & Raga 2000) and thus see their luminosities diminished. In the TF

plot this means that for a given luminosity, V_{\max} shifts to larger values. Observations show that dwarf and normal galaxies have roughly the same infrared TF relation; if anything, dwarf galaxies lie more on the low-velocity side and present more scatter (Pierini & Tuffs 1999; de Jong & Lacey 2000, quoted by Cole et al. 2000, see their Fig. 7). Therefore, the fact that for WDM the small halos are shifted in the $M_v - V_{\max}$ relation as it is shown in Fig. 10 might resolve a potential problem of the CDM scenario. Therefore, it seems that the *WDM scenario could reproduce the infrared TF relation of dwarf galaxies better than the CDM scenarios does.*

5. Unlike in the CDM scenario, for WDM one expects that the satellite dwarf galaxies form later than the host large galaxies. The evolution of the substructure for our WDM simulation Λ WDMt2 ($R_f=0.2$ Mpc) is shown in Table 2. The scale factor normalized to one at present is given in the first column while the number of halos with maximum circular velocity V_{\max} greater than 100 km s^{-1} is presented in column 2. Columns 4, 5, and 6 give the coordinates of the center of mass of the system composed by these halos. The total number of halos with $V_{\max} > 15 \text{ km s}^{-1}$ that contain more than 200 particles and the mass of the most massive halo are given in columns 3 and 7, respectively. We see that the first structure starts to assemble at $z \sim 7$; this seed has a mass of $\sim 3 \times 10^{10} h^{-1} M_\odot$. Later, at $z \sim 4$, when the mass of the most massive halo has grown to $M_v \sim 10^{11} h^{-1} M_\odot$, the first substructures appear by fragmentation. Thus, the building blocks for large galactic and supra-galactic structures are those with masses near to M_f ; smaller structures (guest halos) form slightly later by fragmentation. We may say thus that the formation redshift of guest halos is approximately equal or less than $z_f(M_f)$. For the Λ WDM model with the power spectrum normalized to COBE used here and according to the spherical top-hat model, the typical formation redshift of $\sim 10^{11} h^{-1} M_\odot$ halos is $z_f(10^{11} h^{-1} M_\odot) \approx 1.3$ and 3.7 for $1-\sigma$ and $2-\sigma$ peaks, respectively. If galaxies form from high peaks, then the typical formation redshifts of galaxies of $\sim 10^{11} h^{-1} M_\odot$ will be larger than $z = 2 - 3$. For the Λ WDM models with $R_f \lesssim 0.2$ Mpc, smaller galaxies (dwarfs) will form slightly later than these redshifts. Similar conclusions are obtained by Bode et al. (2000), who also remark that low mass halos form solely within pancakes and filaments, and not in the voids, in contrast to the situation in the CDM scenario (see also Fig. 1).

From the observational point of view, there are some pieces of evidence that dwarf galaxies formed later than bright galaxies. In the Local Group, all dwarf galaxies seem to have their oldest stellar population slightly younger than the oldest Milky Way halo population (Mateo 1998); for the Large Magellanic Cloud this age difference could be of 2 Gyr, according to studies of the horizontal branch morphology of stellar clusters (Olszewski, Suntzeff, & Mateo 1996, and references therein), while for the Small Magellanic Cloud the difference should be even larger since this galaxy seems to be younger than its neighborhood. On the other hand, comparisons of observed and modeled galaxy counts for B dropout galaxies at $3.5 \lesssim z \lesssim 4.5$ suggest that some L_\star galaxies were already in place at $z \approx 4$ but dwarf galaxies may have formed later at $3 \lesssim z \lesssim 4$ (Metcalf et al. 2000), in agreement with predictions of the WDM scenario.

6. The Lyman- α forest is a powerful probe of the linear power spectrum on galactic and sub-galactic scales, upon the understanding that it traces the underlying matter density. Since

in a WDM scenario the small-scales modes are damped out, one might think that the observed Lyman- α forest should not be reproduced by this cosmology. However, because of the efficient power transfer from larger to smaller scales (see §6.1), enough power on small scales is regenerated at $z \approx 3-4$. Narayanan et al. (2000) have shown that WDM models ($\Omega_m = 0.3$ and $\Omega_\Lambda = h = 0.7$) with $R_f \lesssim 0.155$ Mpc ($m_W \gtrsim 0.75$ keV) are able to reproduce the observed properties of the Lyman- α forest. This last point, more than an advantage of WDM with respect to CDM, is a test for the former scenario. The CDM scenario is also able to predict the properties of the Lyman- α forest.

As we have seen, the WDM scenario works better than the CDM one in several aspects. Nonetheless, both scenarios fail in predicting soft halo cores and the independence of the halo central density on its mass, as some inferences from observations seem to suggest (e.g., Firmani et al. 2000a,b and the references therein). More observational data which explore in detail the inner structure of the halo component of galaxies are urgent³; however, it is likely that the more decisive data will come from strong lensing studies of clusters of galaxies (the largest virialized structures). The phase space density of dark matter halos derived from observations also offers an important test for the WDM scenario (Hogan & Dalcanton 2000; Sellwood 2000). If more detailed observational studies confirm the existence of soft halo cores with the scaling properties suggested in Firmani et al. (2000a,b) and Sellwood (2000), the WDM scenario must be abandoned. Then alternatives such as the self-interacting CDM might become more appealing.

7. Summary and conclusions

We have carried out high-resolution N-body cosmological simulations with the aim to study the effect on the halo density profiles produced by (i) the damping of the power spectrum at small scales and (ii) the introduction of a relict thermal velocity dispersion, as well as to explore the viability of the WDM scenario. We have also studied hot monolithic collapse by means of an analytical model and top-hat N-body simulations. Our main conclusions are:

- For the halos studied here, with masses close or up to ~ 100 times smaller than the filtering mass M_f , the density profiles are on average well described by the NFW shape; the density profiles were well resolved down to $\sim 0.01 r_v$. The only differences between halos with masses below M_f and their CDM counterparts is that the former have lower concentrations and their innermost density profiles are not as steep as $r^{-1.5}$. Thus, though the cosmogony of the halos in both cases is different, the final virialized structures are not dramatically different.

- The $c_{1/5}$ or c_{NFW} concentrations of halos more massive than a few times the filtering mass M_f

³ At the time this paper has being refereed, new high resolution rotation curve observations for LSB galaxies were presented by de Blok et al. (2001); they conclude that observations are consistent with constant density halo cores of "modest (~ 1 kpc) core radius, which can give the illusion of steep cusps when insufficiently resolved".

are similar to those of their CDM counterparts. However, as the mass decreases, the concentrations on average remain almost constant (slightly decrease), while for CDM halos the concentration increase monotonically. The scatter of the concentration for a given mass is large in both cases. The difference in the concentrations of the small halos can be explained because the relatively late formation epoch of small halos in the simulations with damped power spectrum at small scales.

-The relict thermal velocity dispersion of warmons, v_{th}^{w} , does not affect the density profiles of WDM halos, at least down to $0.01 r_{\text{v}}$. For our simulations with $R_{\text{f}}=0.2$ and 1.7 Mpc (ΛWDMt2 and ΛWDM_{60} , respectively) we used a thermal velocity two times larger than v_{th}^{w} and we did not find any significant difference in the halo concentrations and density profiles with respect to the case with $v_{\text{th}}=0$. For the high-resolution run ΛWDM_{60} we also experimented with $v_{\text{th}}=4$ and 16 times v_{th}^{w} , finding resolved soft cores only for the last case (with radii at $\sim 0.03 - 0.04 r_{\text{v}}$).

-The inner structure of dark matter halos formed through monolithic collapse can be affected *only* if the particles have a significant (tangential) velocity dispersion v_{rms} . The penetration degree towards the halo center is determined by the pericenter of the orbiting particle, or equivalently, the angular momentum forces the particles to avoid migration towards inner regions. From N-body simulations of the collapse of top-hat spheres with different amounts of v_{th} , we have found that the core radius scales linearly with v_{th} up to velocities much larger than v_{th}^{w} . In order that WDM halos with masses close to M_{f} form noticeable cores, v_{th} should be much larger than v_{th}^{w} .

We conclude that a flat ΛWDM model with $R_{\text{f}} \approx 0.16$ Mpc ($m_{\text{W}} \approx 750$ eV), $\Omega_{\Lambda} \approx 0.7$, and $h \approx 0.7$, has several advantages over its CDM model counterpart. The problem of excess of substructure is solved (Paper I), the halos of dwarf and LSB galaxies are less concentrated than in the CDM scenario as observations suggest (Fig. 9), and the disk angular momentum problem is alleviated (Sommer-Larsen & Dolgov 2000). Furthermore, our preferred WDM model describes better than CDM the TF relation of dwarf galaxies (Fig. 10) and the formation epochs of these galaxies (§6), as well as their large-scale distribution (Bode et al. 2000). On the other hand, this model is not apparently in conflict with measurements of the power spectrum of Lyman- α forest (Narayanan et al. 2000) and with the reionization constraints (Bode et al. 2000). Nonetheless, the WDM model is ruled out if more observations confirm the existence of soft halo cores as well as the independence on mass of their densities; the crucial test is at cluster scales. No doubt, exciting questions remain to be answered in the near future.

We are grateful to A. Klypin and A. Kravtsov for kindly providing us a copy of the ART code in its version of multiple mass, and to H. Couchman for having made available his adaptive P3M-SPH code HYDRA. We also thank A. Klypin for enlightening discussions. We thank the second referee for a throughout and accurate revision of the manuscript as well as for the suggestions which helped to improve the quality of this paper. The first referee is acknowledged for his (her) criticism that conducted us to carry out more simulations in order to study the influence of thermal velocity on halo density profiles. This work has received partial funding from CONACyT grant J33776-E to V.A. The work of E.D. was supported by Fondazione Cariplo, Italy. Our ART simulations

were performed at the Dirección General de Servicios de Cómputo Académico, UNAM, using an Origin-2000 computer.

REFERENCES

- Aguilar, L., Merritt, D. 1990, *ApJ*, 354, 33
- Avila-Reese, V., & Firmani, C. 2000, *RevMexA&A*, 36, 23
- Avila-Reese, V., Firmani, C., & Hernández, X. 1998, *ApJ*, 505, 37
- Avila-Reese, V., Firmani, C., Klypin, A., & Kravtsov, A.V. 1999, *MNRAS*, 310, 527
- Bagla, J.S., & Padmanabhan, T. 1997, *MNRAS*, 286, 1023
- Bardeen, J.M., Bond, J.R., Kaiser, N., & Szalay, A.S. 1986, *ApJ*, 304, 15
- Blumenthal, G.R., Pagels, H., & Primack, J.R. 1982, *Nature*, 299, 37
- Bode, P., Ostriker, J.P., & Turok, N. 2000, preprint (astro-ph/0010389)
- Bullock, J. S., Kravtsov, A.V., & Weinberg, D.H. 2000, *ApJ*, 539, 517
- Burkert, A. 1995, *ApJ*, 477, L25
- Carlberg, R.G., Yee, H.K.C., Ellingson, E., Abraham, R., Gravel, P., Morris, S., Pritchet, C.J. 1996, *ApJ*, 462, 32
- Cole, S., Lacey, C.G., Baugh, C.M., & Frenk, S.F. 2000, preprint (astro-ph/0007281)
- Colín, P., Avila-Reese, V., & Valenzuela, O. 2000, *ApJ*, 542, 622 (Paper I)
- Colombi, S., Dodelson, S., & Widrow, L.M. 1996, *ApJ*, 458, 1
- Couchman, H.M.P, Thomas, A., & Pearce, F.R. 1995, *ApJ*, 452, 797
- de Blok W.J.G., & McGaugh S.S., 1997, *MNRAS*, 290, 533
- de Blok W.J.G., McGaugh S.S., Bosma A., & Rubin V.C., 2001, *ApJ*, in press (astro-ph/0103102)
- Doroshkevich, A.G., Kotok, E.V., Novikov, I.D., Polyudov, A.N., Shandarin, S.F., & Sigov, Yu. S. 1980, *MNRAS*, 192, 321
- Eke, V.R., Cole, S., Frenk, C.S., & Henry, P.J. 1998, *MNRAS*, 298, 1145
- Firmani, C., & Avila-Reese, V. 2000, *MNRAS*, 315, 457
- Firmani, C., D’Onghia, E., Avila-Reese, V., Chincarini, G., & Hernández, X. 2000a, *MNRAS*, 315, L29
- Firmani, C., D’Onghia, E., Chincarini, G., Hernández, X., & Avila-Reese, V. 2000b, *MNRAS*, 321, 713

- Flores, R., & Primack, J.R. 1994, *ApJ*, 427, L1
- Frenk, C.S., White, S.D.M., Davis, M., & Efstathiou, G. 1988, *ApJ*, 327, 507
- Hannestad, S., & Scherrer, R.J. 2000, *Phys.Rev.* D62, 043522
- Hogan, C.J. 1999, preprint (astro-ph/9912549)
- Hogan, C.J., & Dalcanton, J.J. 2000, *Phys.Rev.* D62, 063511
- Huss, A., Jain, B., Steinmetz, M. 1999, *ApJ*, 517, 64
- Tremaine, S., & Gunn, J.E. 1979, *Phys.Rev.Lett.* 42, 407
- Kamionkowski, M., & Liddle, A.R. 1999, preprint (astro-ph/9911103)
- Kauffmann, G., White, S. D. M., & Guideroni, B. 1993, *MNRAS*, 264, 201
- Klypin, A.A., Kravtsov, A.V., Valenzuela, O., Prada, F. 1999, *ApJ*, 522, 82
- Klypin, A.A., & Holtzman, J. 1997, preprint (astro-ph/9712217)
- Klypin, A.A., Kravtsov, A.V., Bullock, J., & Primack, J. 2000, preprint (astro-ph/0006343)
- Kravtsov, A.V., Klypin, A.A., & Khokhlov, A.M. 1997, *ApJS* 111, 73
- Lin, W.B., Huang, D.H., Zhang, X., & Brandenberger, R. 2001, *Phys.Rev.Lett.* 86, 954
- Little, B., Weinberg, D.H., & Park, Ch. 1991, *MNRAS*, 253, 295
- Mac Low, M.-M., & Ferrara, A. 1999, *ApJ*, 513, 142
- Mateo, M. L. 1998, *ARA&A*, 36, 435
- Melott, A.L., & Shandarin, S.F. 1990, *Nature*, 346, 633
- Metcalf, N., Shanks, T., Campos, A., McCracken, H.J., & Fong, R. 2000, preprint (astro-ph/0010153)
- Mo, H.J., Mao, S., & White, S.D.M. 1998, *MNRAS*, 295, 319
- Moore, B. 1994, *Nature*, 370, 629
- Moore, B., Ghigna, S., Governato, F., Lake, G., Quinn, T., Stadel, J., & Tozzi, P. 1999a, *ApJ*, 524, L19
- Moore, B., Quinn, T., Governato, F., Stadel, J., & Lake, G. 1999b, *MNRAS*, 310, 1147
- Narayanan, V.K., Spergel, D.N., Davé, R., & Ma, Ch-P. 2000, *ApJ*, 543, L103

- Navarro, J.F., Frenk, C.S., & White, S.D.M. 1997, *ApJ*, 490, 493
- Olszewski, E.W., Suntzeff, N.B., & Mateo, M. 1996, *ARA&A*, 34, 511
- Pierini, D., & Tuffs, R.J. 1999, *A&A*, 343, 751
- Pierpaoli, E., Borgani, S., Masiero, A., & Yamaguchi, M. 1998, *Phys.Rev.D*, 57, 2089
- Shapiro, P.R., & Raga, A.C. 2000, in “Astrophysical Plasmas: codes, models, and observations”, eds. J. Arthur, N. Brickhouse, & J. Franco, *RevMexA&A Serie de Conferencias*, 9, 292
- Sellwood, J.A. 2000, *ApJ*, 540, L1
- Sommer-Larsen, J., & Dolgov, A. 2000, *ApJ*, 551, 608
- Steinmetz, M., & Navarro, J.F. 1999, *ApJ*, 513, 555
- Swaters, R.A., Madore, B.F., & Trewhella, M. 2000, *ApJ*, 531, L107 in press (astro-ph/0001277)
- Tittley, E.R., & Couchman, H.M.P. 1999, preprint (astro-ph/9911365)
- Valinia, A., Shapiro, P.R., Martel, H., Vishniac, E.T. 1997, *ApJ*, 479, 46
- van den Bosch, F.C., & Swaters, R.A. 2000, preprint (astro-ph/0006048)
- van den Bosch, F., Robertson, B.E, Dalcanton, J.J, & de Blok, W.J.G. 1999, *AJ*, 119, 1579
- White, M., & Croft, R.A.C. 2000, *ApJ*, 539, 437
- Zel’dovich, Y.B. 1970, *A&A*, 5, 84

Table 1. Models and Simulations Parameters

Run	R_f (Mpc)	M_f $h^{-1}M_\odot$	v_{th}^a ($\times v_{\text{th}}^w$)	m_p ($h^{-1}M_\odot$)	Box ($h^{-1}\text{Mpc}$)	Resolution ($h^{-1}\text{kpc}$)	N_{host}
ΛWDM	0.2	2.9×10^{11}	0.0	2.1×10^6	7.5	0.1	1
$\Lambda\text{WDM}_{7.5}$	1.7	1.7×10^{14}	0.0	2.1×10^6	7.5	0.4	1
ΛWDM_{15}	1.7	1.7×10^{14}	0.0	1.7×10^7	15.0	0.4	1
ΛWDM_{30}	1.7	1.7×10^{14}	0.0	1.3×10^8	30.0	1.8	4
ΛWDM_{60}	1.7	1.7×10^{14}	0.0	1.1×10^9	60.0	1.8	4
ΛCDM_{60}	0.0	0.0	0.0	1.1×10^9	60.0	1.8	4
ΛWDMt2	0.2	2.9×10^{11}	2	2.1×10^6	7.5	0.1	1
$\Lambda\text{WDM}_{60\text{t}2}$	1.7	1.7×10^{14}	2	1.1×10^9	60.0	1.8	4
$\Lambda\text{WDM}_{60\text{t}4}$	1.7	1.7×10^{14}	4	1.1×10^9	60.0	1.8	4
$\Lambda\text{WDM}_{60\text{t}16}$	1.7	1.7×10^{14}	16	1.1×10^9	60.0	1.8	4

^aThermal velocity dispersion added to the particles at $z = 40$, in units of the relic thermal velocity corresponding to the warmion mass used in the simulation, v_{th}^w

Table 2. Substructure evolution in model ΛWDMt2

Epoch	$N_{h,100}$	N_N	X_{cm} ($h^{-1}\text{Mpc}$)	Y_{cm} ($h^{-1}\text{Mpc}$)	Z_{cm} ($h^{-1}\text{Mpc}$)	M_v ($h^{-1}M_\odot$)
1.000	1	13	7.193	5.236	1.406	1.4×10^{12}
0.879	1	11	7.191	5.287	1.424	1.3×10^{12}
0.753	1	17	7.175	5.349	1.443	1.1×10^{12}
0.630	2	24	7.153	5.453	1.452	6.6×10^{11}
0.504	4	24	7.191	5.454	1.626	5.2×10^{11}
0.405	4	29	7.139	5.705	1.516	4.9×10^{11}
0.354	5	26	7.155	5.740	1.528	2.9×10^{11}
0.303	4	20	7.170	5.875	1.472	2.4×10^{11}
0.255	3	15	0.379	5.837	1.515	1.8×10^{11}
0.204	2	6	7.117	6.623	1.055	1.1×10^{11}
0.153	2	2	7.135	6.148	1.406	5.2×10^{10}
0.129	1	1	7.151	6.994	0.650	2.7×10^{10}

Fig. 1(a).— Distribution of dark matter particles in run Λ WDM₆₀ inside a cube of $40 h^{-1}\text{Mpc}$ comoving on a side at different epochs: $a = 0.3, 0.5, 0.75$, and 1.0 , where a is the scale factor. All particles that are within a sphere of radius $1.5 h^{-1}\text{Mpc}$ centered on a host halo at $a = 1$ were traced back to the chosen epoch and their center of mass was computed. Cubes were then centered on these centers of masses. We have color-coded particles on a gray scale according to the logarithm of their local density (a *pgplot* program kindly provided by A. Kravtsov). The local density at the particle positions, on the other hand, was computed using SMOOTH, a publicly available code developed by the HPC group in the University of Washington Department of Astronomy.

Fig. 1(b).— Same as (a), but for CDM, run Λ CDM₆₀.

Fig. 1.— (c). *Right panel:* Distribution of dark matter particles inside a sphere of radius $1.5 h^{-1}\text{Mpc}$ centered on the large host halo seen in plot 1(a) at $a = 1$. The mass of the selected host halo is about half the corresponding filtering mass ($M_f = 1.7 \times 10^{14} h^{-1}M_\odot$), and it was one of the first structures to collapse in the simulation. *Left panel:* Same particles of right panel but traced back to $a = 0.5$. All of them lie within a sphere of radius $5.6 h^{-1}\text{Mpc}$ comoving centered on the center of mass of the particle system at this epoch.

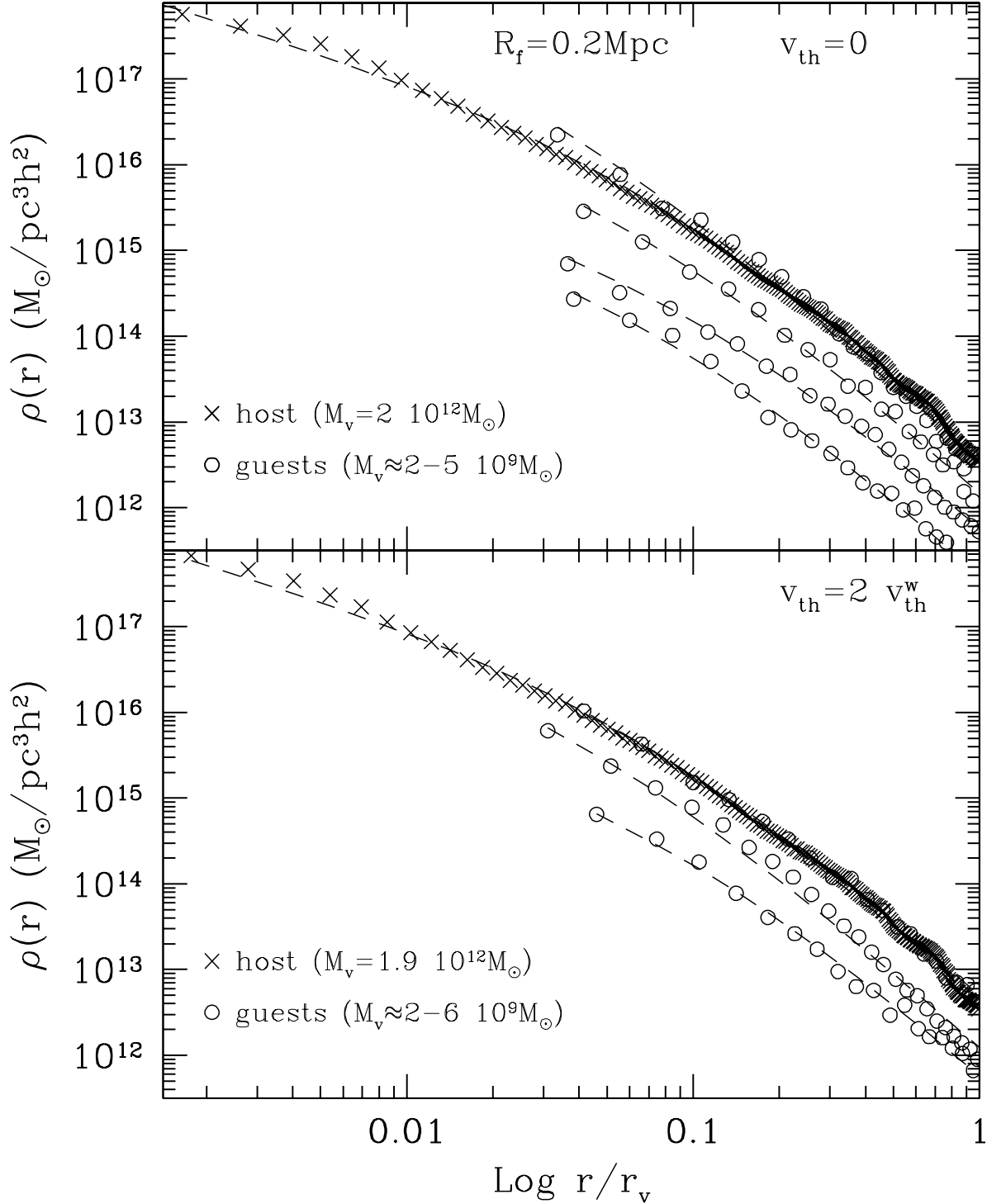


Fig. 2.— Density profiles of the host (crosses) and guest halos with more than 1000 particles (circles) from Λ WDM simulations with $R_f = 0.2$ Mpc ($m_W = 605$ eV) with zero thermal velocity dispersion (upper panel, run Λ WDM) and with a thermal velocity dispersion twice larger than that corresponding to a warmion of 605 eV (lower panel, run Λ WDMt2). Radii are normalized to the current halo virial radius r_v . The inner point in each plotted profile is the maximum of 4 times the formal force resolution (Table 1) and the radius of the first point containing more than 50 particles.

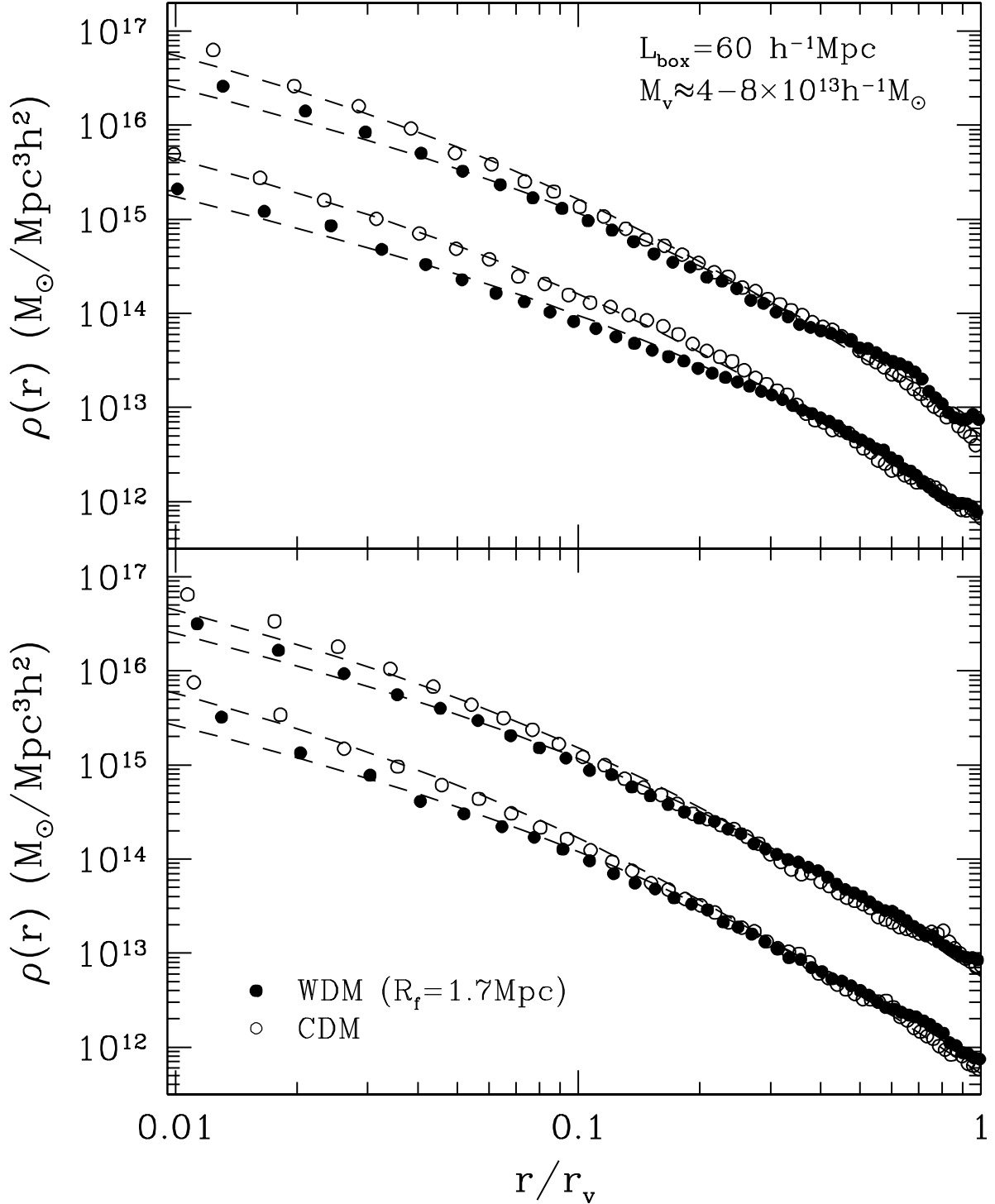


Fig. 3.— Density profiles of the four host halos in simulations Λ WDM₆₀ (solid circles) and Λ CDM₆₀ (empty circles). In order to prevent visual confusion, two panels are used and the two lower profiles in each 0panel were shifted by -1 in the log. The dashed lines are NFW fits to these profiles. The inner points and the normalization of the radius are as in Fig. 2. The masses of the WDM halos are 2-4 times smaller than the filtering mass $M_f = 1.7 \times 10^{14} h^{-1} M_\odot$.

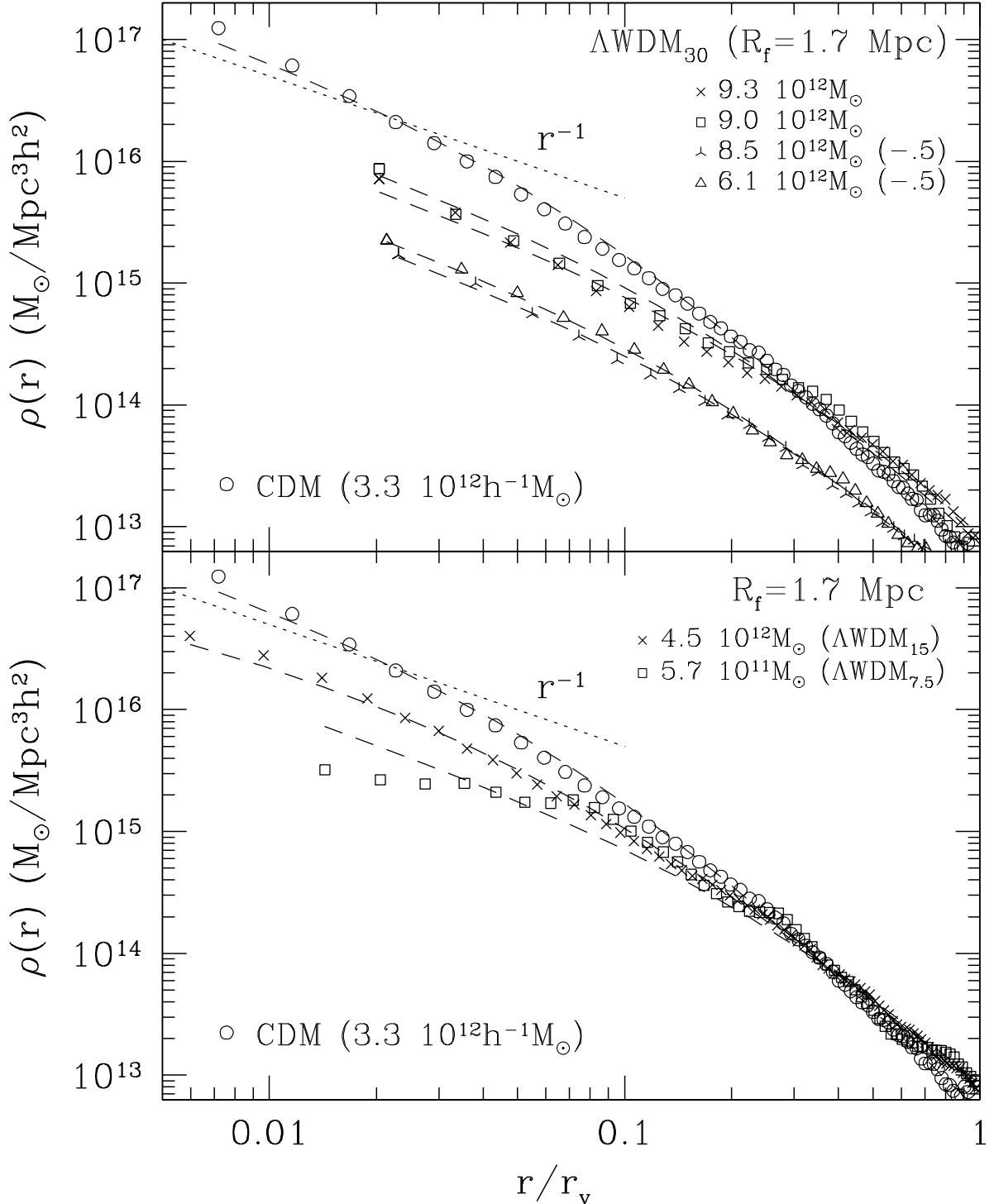


Fig. 4.— *Upper panel:* Density profiles of the four host halos from simulation ΛWDM_{30} . The two lower profiles were shifted by -0.5 in the log in order to avoid overlapping. Dashed lines are the best NFW fit. For comparison, the profile of a CDM halo from Paper I is also plotted (empty circles). The inner points and the normalization of the radius are as in Fig. 2. *Lower panel:* The same as the upper panel but for the two host halos from runs ΛWDM_{15} (crosses) and $\Lambda\text{WDM}_{7.5}$ (squares), respectively. As one expects, the density profile of the halo from run $\Lambda\text{WDM}_{7.5}$ is affected by the small size of the box (see §3).

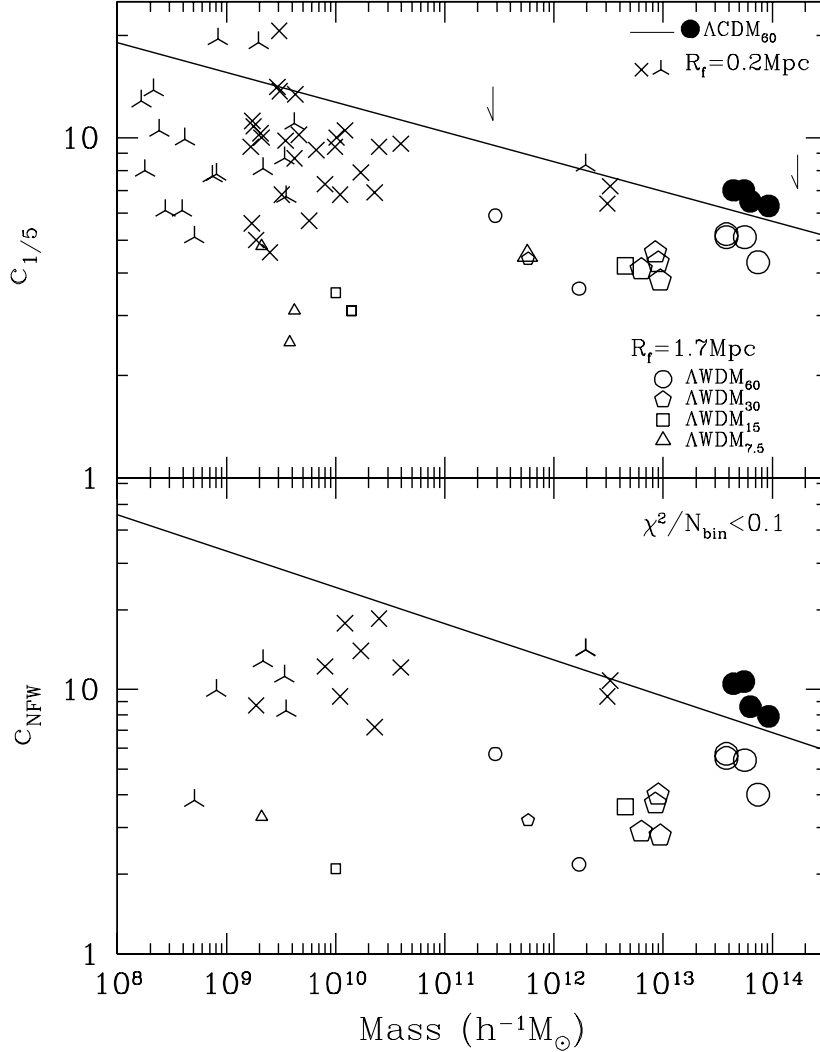


Fig. 5.— Concentration parameters $c_{1/5}$ and c_{NFW} vs. halo virial mass (*upper* and *lower* panels respectively) from the ΛWDM simulations with $R_f=1.7$ Mpc (empty symbols) and $R_f=0.2$ Mpc (crosses and skeletal triangles, from Paper I, and from the model ΛWDM presented here, respectively), and from the ΛCDM_{60} simulation (solid circles). Large empty symbols are for the corresponding host halos, while small empty symbols are for the guest halos with more than 1000 particles; they are only a few. The solid line is a linear fit for thousands of isolated halos obtained in a ΛCDM simulation (Avila-Reese et al. 1999). The vertical arrows indicate the filtering masses M_f corresponding to $R_f=0.2$ and 1.7 Mpc. The c_{NFW} parameter for the guest halos in the simulations of Paper I and the model ΛWDMt2 presented here are shown only for those halos whose profiles fit the NFW shape with an accuracy better than $D < 10\%$. Note that the concentration parameters of halos below M_f remain almost constant as the mass decreases while in the case of the CDM model these concentrations continuously increase as the mass decreases.

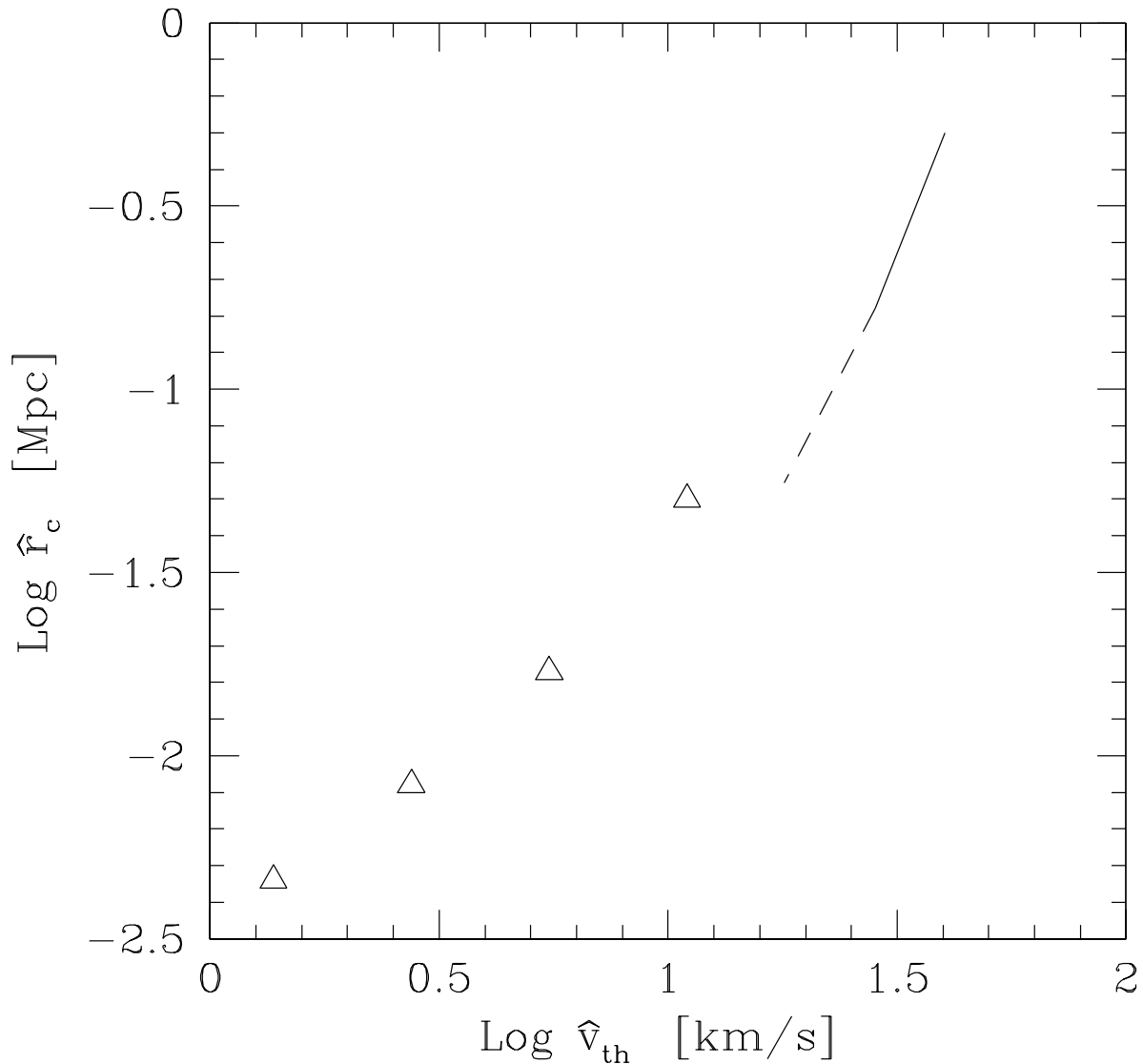


Fig. 6.— Core radii obtained in N-body simulations of monolithic collapse with increasing values of thermal velocity (triangles) and predicted by the analytical model (line, see text). The dashed part of the line is at values of thermal velocity where the analytical model begins to lose its validity.

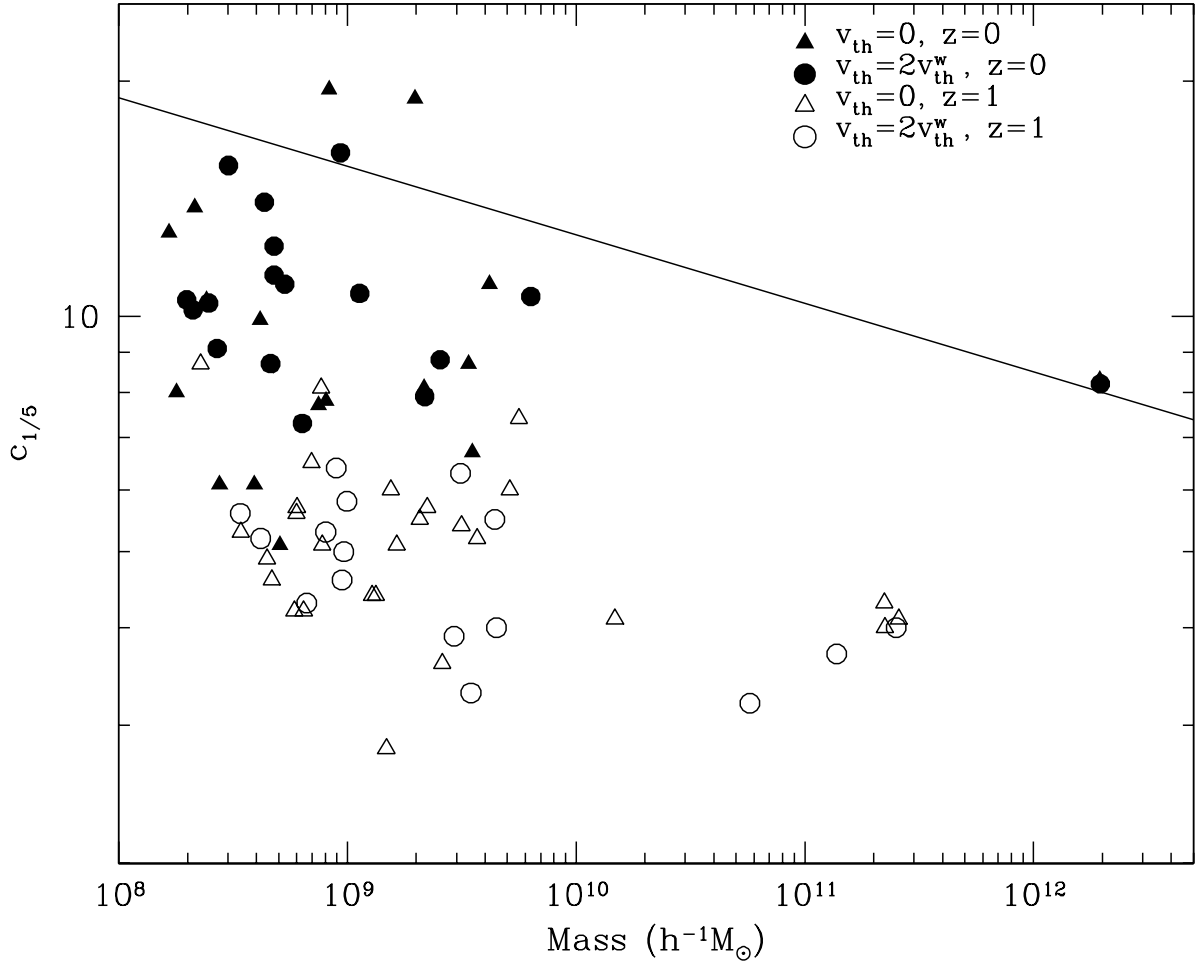


Fig. 7.— Concentration parameter $c_{1/5}$ vs. halo mass from Λ WDM simulations ($R_f=0.2$ Mpc, $L_{\text{box}} = 7.5h^{-1}\text{Mpc}$) with $v_{\text{th}}=0$ (run Λ WDM triangles) and with $v_{\text{th}}=6.7 \text{ km s}^{-1}$ determined at $z_i = 40$ (run Λ WDMt2 circles); this velocity is two times larger than the corresponding v_{th}^w . The filled symbols are for halos at $z = 0$ while the empty symbols are for halos at $z = 1$. There is not any significant difference in between simulations with and without thermal velocity inclusion.

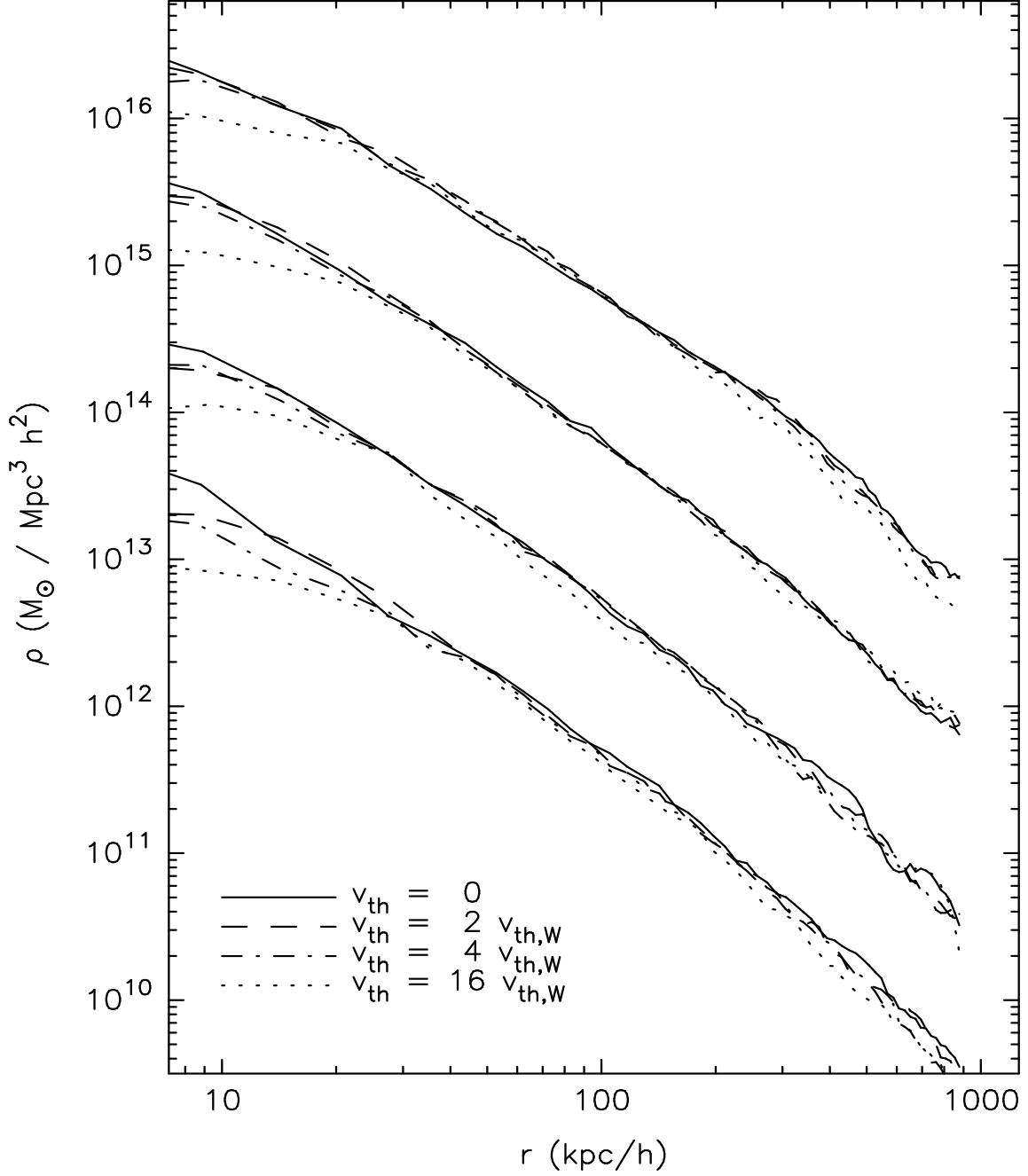


Fig. 8.— Density profiles of the four host halos re-simulated in the Λ WDM simulations with $R_f=1.7$ Mpc and $v_{\text{th}}=0$ (solid line, run ΛWDM_{60} , see also Fig. 2), $v_{\text{th}}=2v_{\text{th}}^{\text{w}}$ (dashed line, run $\Lambda\text{WDM}_{60\text{t}2}$), $v_{\text{th}}=4v_{\text{th}}^{\text{w}}$ (dot-dashed line, run $\Lambda\text{WDM}_{60\text{t}4}$), and $v_{\text{th}}=16v_{\text{th}}^{\text{w}}$ (solid line, run $\Lambda\text{WDM}_{60\text{t}16}$). The velocity v_{th}^{w} is that corresponding to a warmon of 124 eV. The profiles were shifted vertically by 1 in the log in order to avoid overlapping. Soft cores larger than $\sim 0.01 r_{\text{v}}$ appear only when the dispersion velocities are much larger than the warmon thermal velocities.

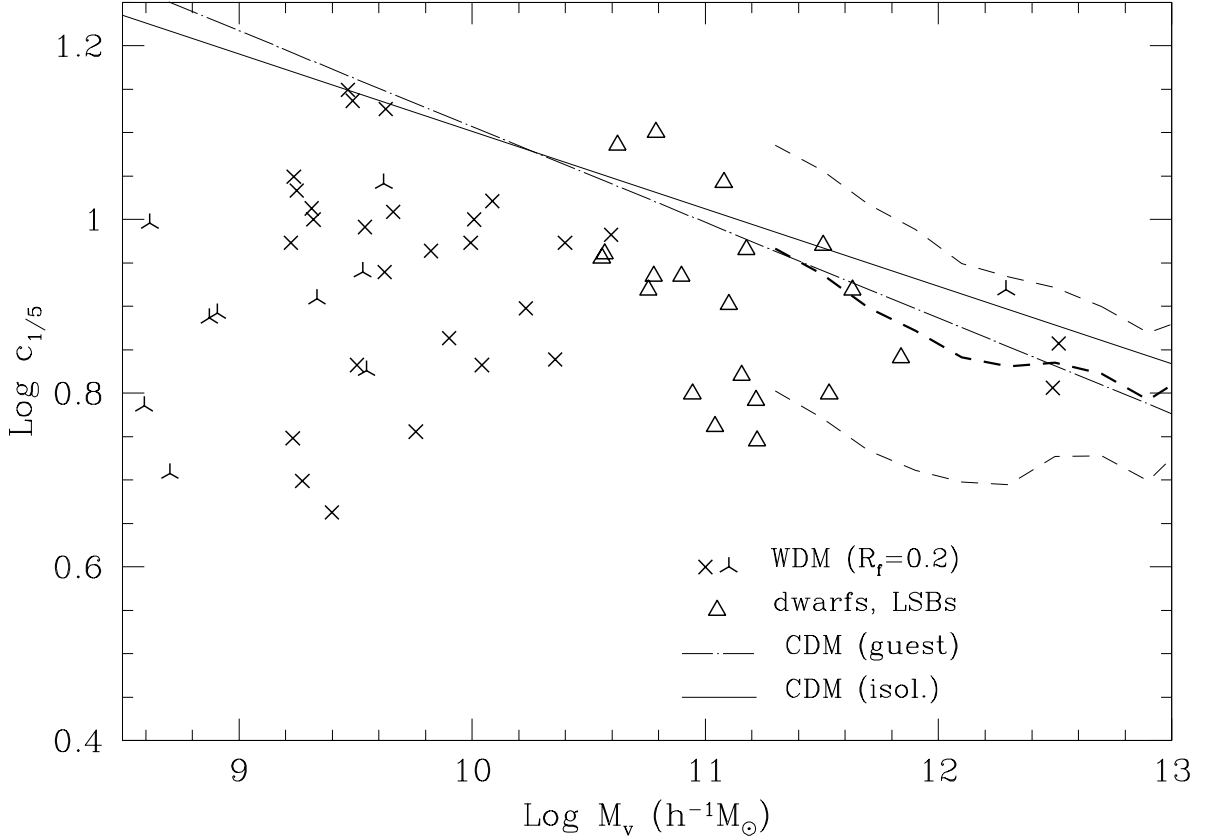


Fig. 9.— Comparison of the $c_{1/5}$ concentration parameters of Λ WDM halos ($R_f=0.2$ Mpc, crosses and skeletal triangles) with those inferred from the rotation curves of dwarf and LSB galaxies (triangles). Crosses correspond to a run presented in Paper I ($L_{\text{box}} = 15h^{-1}\text{Mpc}$, while skeletal triangles are from the run Λ WDM presented here ($L_{\text{box}} = 7.5h^{-1}\text{Mpc}$). The dashed lines are the average concentrations and standard deviations of guest halos found in a Λ CDM simulation (Avila-Reese et al. 1999). The dot-dashed line is a linear fit to these data, while solid line is the linear fit to data corresponding to isolated halos in the same simulation. The observational data for dwarf galaxies were taken from van den Bosch & Swaters 2000 who fit the halo component of their rotation curve decompositions to a NFW profile finding this way c_{NFW} . We pass from c_{NFW} to $c_{1/5}$ and take into account the difference in the definition of virial radius of van den Bosch & Swaters with our definition (the difference in $c_{1/5}$ is not more than a factor of 1.05 larger with our definition respecting that of these authors). The mass of the halos is calculated from the V_{200} reported by them: $M_v[h^{-1}M_{\odot}] = 4.2 \times 10^5 V_{200}^3 [\text{km s}^{-1}]$. We have used only those galaxies for which a meaningful fit to the NFW is found. For the LSB galaxies, data from van den Bosch et al. 2000 were used. The same procedure described for the dwarf galaxies was used. We have considered only those galaxies for which the estimated V_{200} is smaller than the measured V_{max} . Unfortunately, WDM models and observations do not overlap too much. Nevertheless, one already sees that the halos of dwarf and LSB galaxies are in average less concentrated than the CDM ones, being in better agreement with the WDM halos.

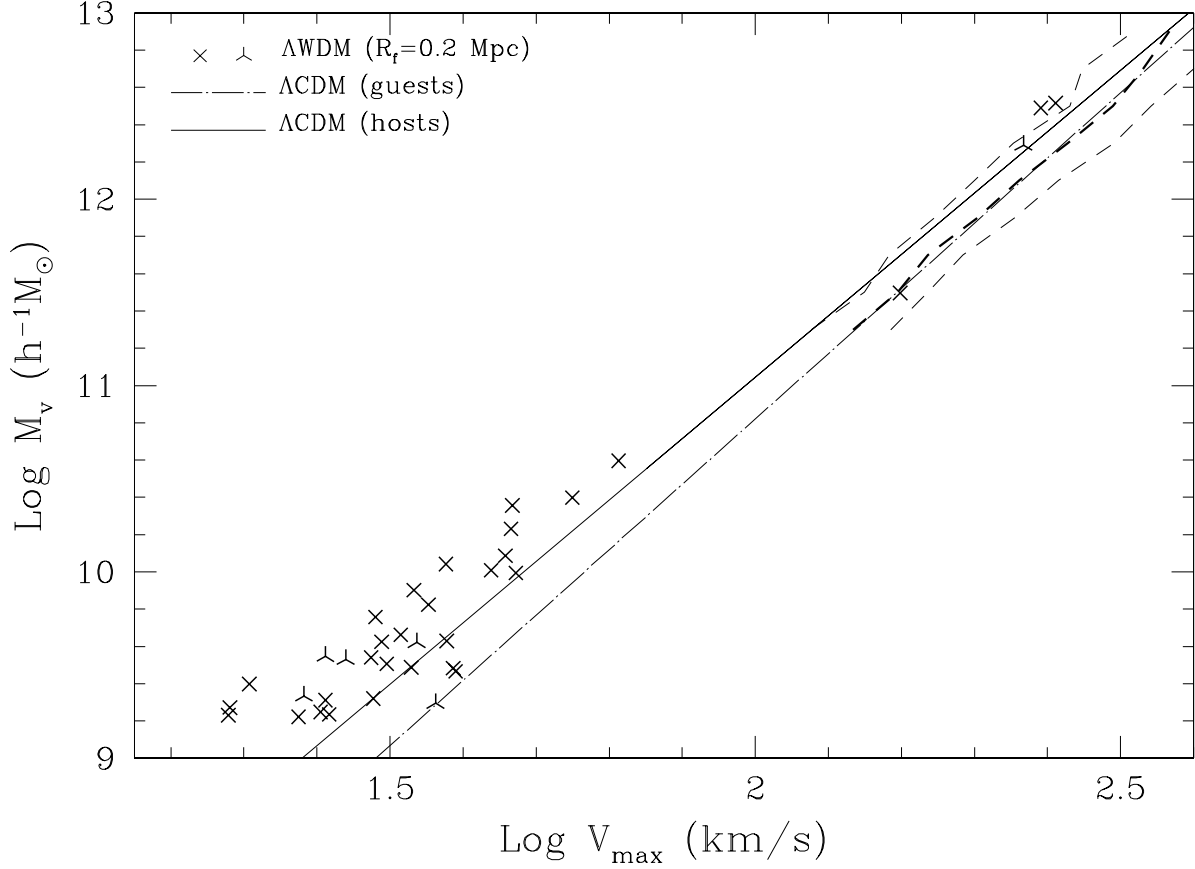


Fig. 10.— Halo mass vs. its maximum circular velocity for the same runs presented in Fig. 4 and 6 (Λ WDM model with $R_f=0.2$ Mpc; crosses and skeletal triangles). For comparison, we also plot the mass-velocity relation and its dispersion for guest halos (dashed lines) found in a Λ CDM simulation, a linear fit to this relation (dot-dashed line), and a linear fit corresponding to isolated halos (solid line) (see Avila-Reese et al. 1999).

This figure "Fig01a.jpg" is available in "jpg" format from:

<http://arxiv.org/ps/astro-ph/0010525v3>

This figure "Fig01b.jpg" is available in "jpg" format from:

<http://arxiv.org/ps/astro-ph/0010525v3>

This figure "Fig01c.jpg" is available in "jpg" format from:

<http://arxiv.org/ps/astro-ph/0010525v3>